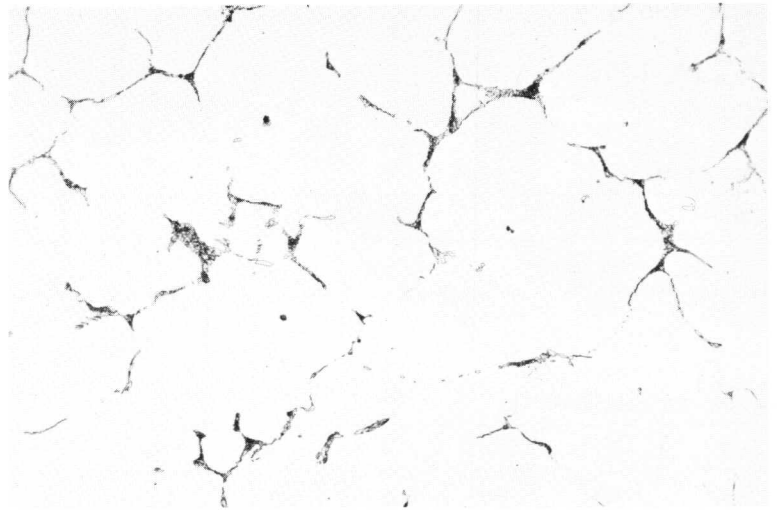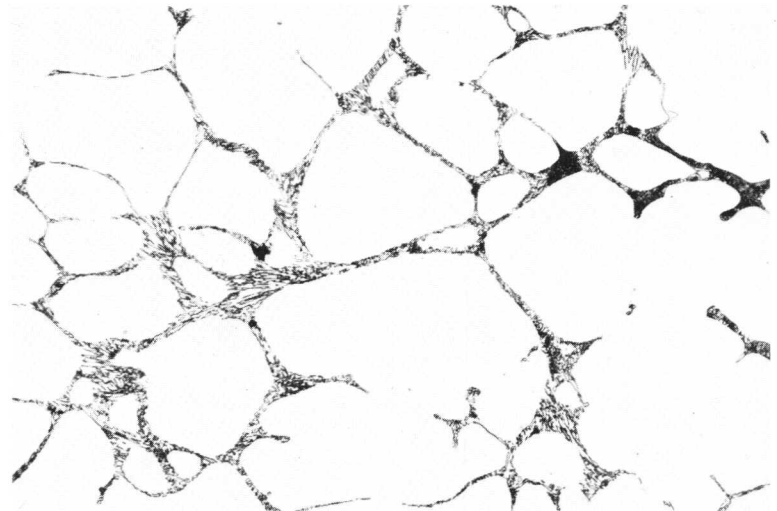**Figure 9**
R   = 2,0°C/s
Tq = 1230°C
11,4 vol-% $M_{23}C_6$.

× 150   100 μm

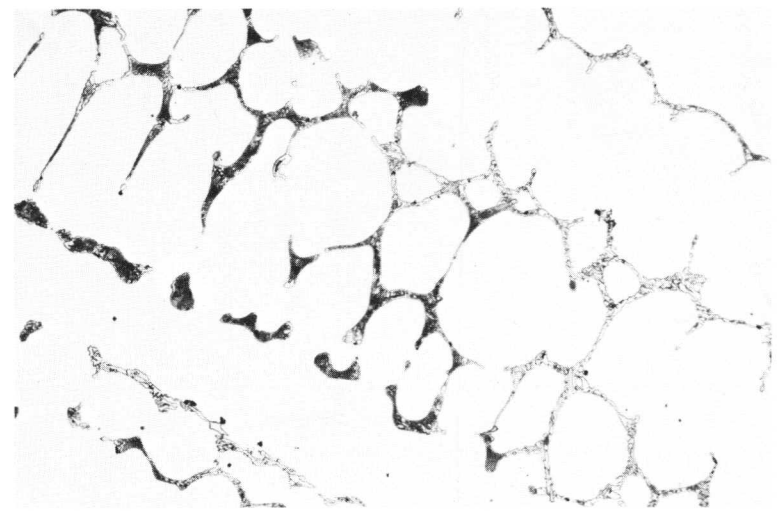
Figure 10
R   = 0,5°C/s
Tq = 1230°C
8,0 vol-% $M_{23}C_6$.

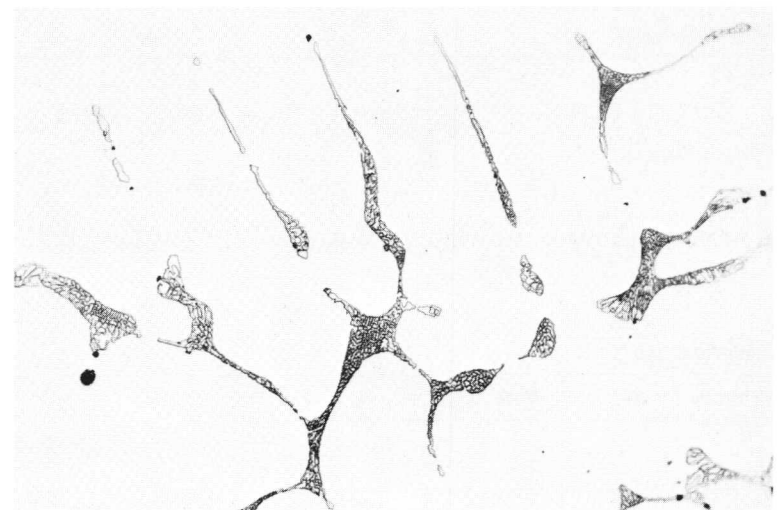× 150   100 μm

Figure 11
R   = 0,5°C/s
Tq = 1100°C
10,7 vol-% $M_{23}C_6$.

× 150   100 μm

Figure 12
R   = 0,1°C/s
Tq = 1230°C
7,2 vol-% $M_{23}C_6$.

× 150   100 μm

STEEL 415. 0,07 % C 21 % Cr 31 % Ni   STAINLESS AND HEAT RESISTANT STEEL
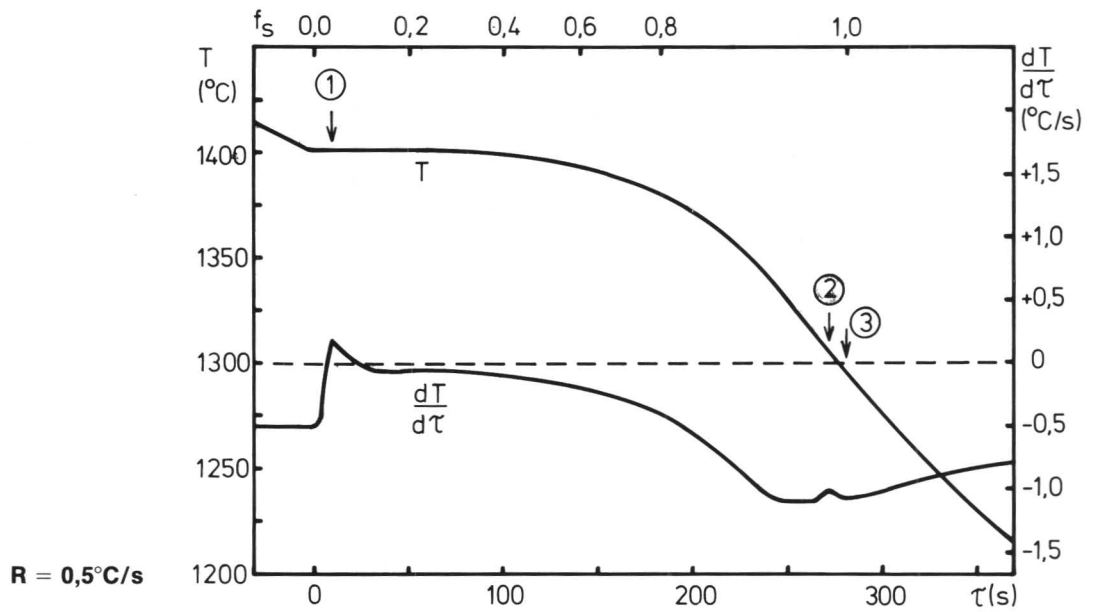
Designations

SIS	AISI	Werkstoff Nr
—	Alloy 800	1.4876

Composition (wt–%)

C	Si	Mn	P	S	Cr	Ni	Mo	Cu	Co	Ti	Al_{tot}	N
0,07	0,62	0,56	0,007	0,003	21,1	30,9	0,06	0,02	0,02	0,40	0,39	0,019

$$\frac{Cr_{eq}}{Ni_{eq}} = 0,71$$

Thermal Analysis

R = 0,5°C/s

	Average Cooling Rate, R, (°C/s)		
	2,0	0,5	0,1
Liquidus temperature, austenitic primary phase, °C ①	1399	1401	1400
Temperature of formation of titanium compounds, °C ②	1305 – 1280	1310 – 1295	1350 – 1330
Solidus temperature, °C ③	1280	1295	1330
Solidification range, °C	120	105	70
Solidification time, s	125	280	810

Precipitates

Ti (C,N) and sulphides containing titanium, (see figures 6 and 7).

Microsegregation

Element	Si	Mn	Cr	Ni
I	2,3	1,7	1,2	1,1

R = 0,5 °C/s
Tq = 1290 °C

Partly solidified

Figure 1
R   = 0,5°C/s
Tq = 1390°C
d   = 80 µm
γ-dendrites and quenched liquid (L).

× 25   400 µm
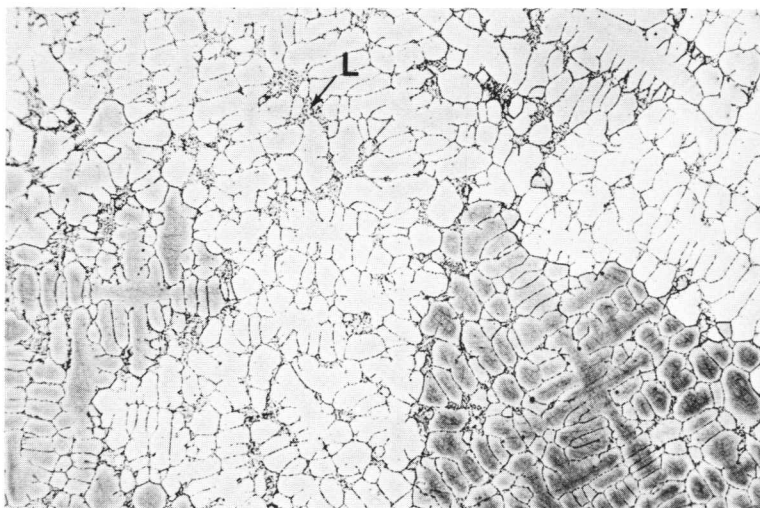
Completely solidified

Figure 2
R   = 2,0°C/s
Tq = 1280°C
d   = 50 µm
Figures 2−4: γ-dendrites.

× 25   400 µm

Figure 3
R   = 0,5°C/s
Tq = 1290°C
d   = 95 µm
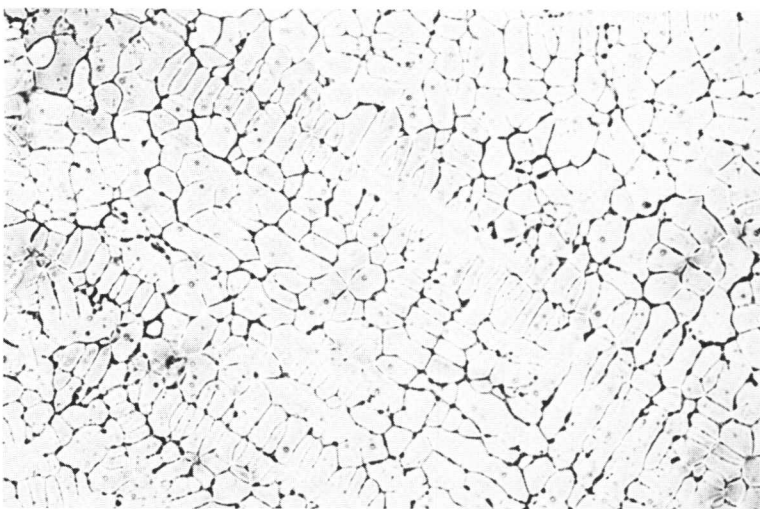
× 25   400 µm

Figure 4
R   = 0,1°C/s
Tq = 1290°C
d   = 145 µm

× 25   400 µm
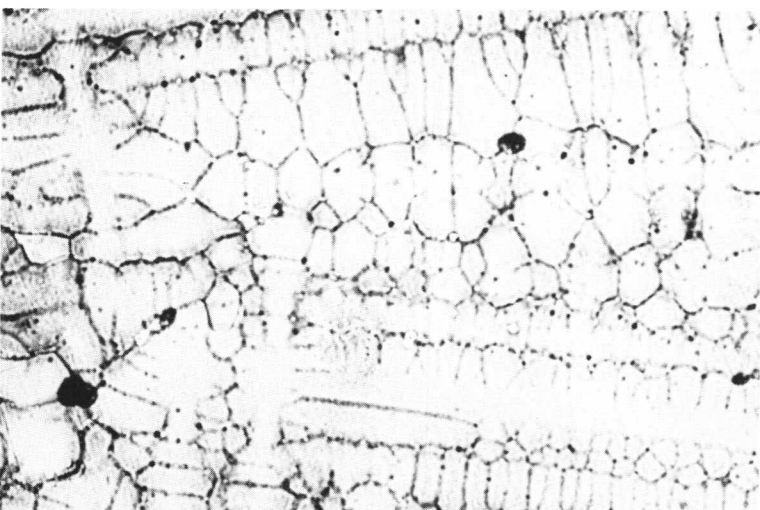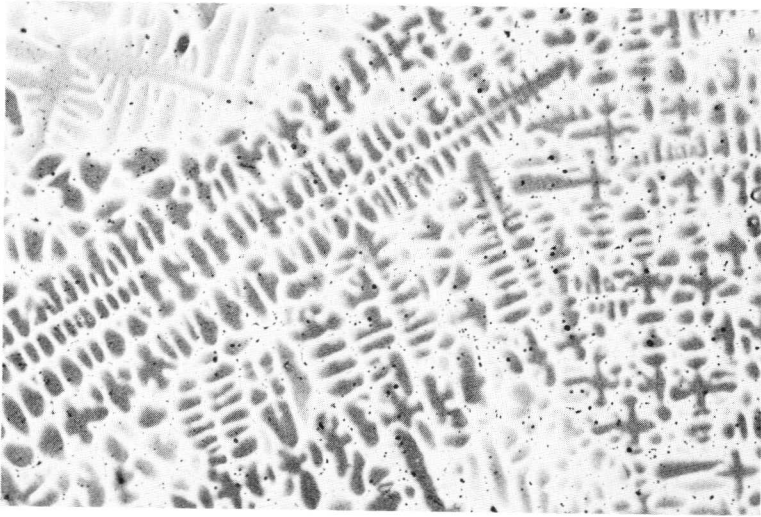
Figure 5

R = 0,5°C/s
Tq = 1200°C
(d_{1200} = 105 μm)
γ-dendrites (dark).

400 μm   × 25
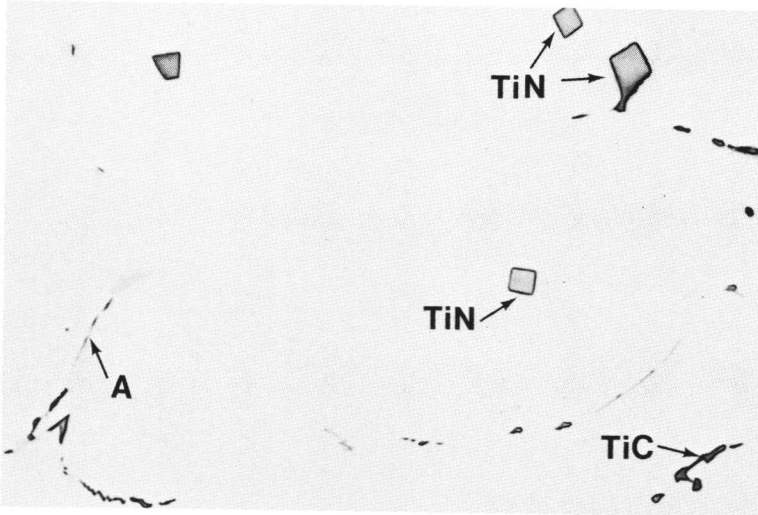
Figure 6

R = 0,5°C/s
Tq = 1290°C
TiN, TiC and sulphides containing titanium (A).
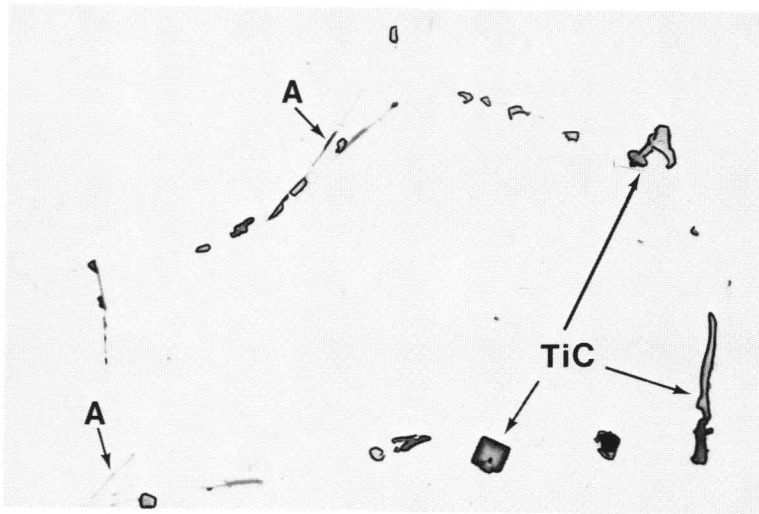
25 μm   × 600

Figure 7

R = 0,5°C/s
Tq = 1200°C
TiC and sulphides containing titanium (A).

25 μm   × 600

5. High Speed Steels

High speed steels are highly alloyed tool steels which exhibit enhanced hardness and wear resistance at high temperatures. These steels have a high carbon content and varying amounts of chromium, molybdenum, tungsten and vanadium.

The wide solidification ranges and microsegregation of alloying elements in these steels limit their production to small ingots for rolling and forging. Continuous casting is not practised. Considerable use is made of powder metallurgical methods to produce homogeneous, isotropic material.

Although the solidification of high speed steels has been studied in great detail for many years, they were included in the present study for the sake of uniformity and for comparison with other alloys. The two most common commercial high speed steels were chosen, with chemical compositions according to table 5.1:

No.	C	Si	Mn	Cr	Ni	Mo	W	V %
501	0,9	0,3	0,3	3,9	0,4	4,9	6,1	1,9
502	1,0	0,4	0,4	3,8	0,1	9,2	1,5	2,0

Table 5.1 High speed steels

The pseudobinary equilibrium phase diagram in figure 5.1 illustrates schematically the complicated solidification sequence, which is roughly the same for both steels. The following reactions take place in order with falling temperature:

● primary ferrite formation
● peritectic reaction and transformation producing austenite
● eutectic reaction producing austenite and carbides

The distinction, used in this work, between peritectic reaction and transformation is defined in chapter 4.

References

General investigations of the solidification of high speed steels dealing with development of the structure, constitution and reaction mechanisms have been reported, [87–95]. Quantitative data on microsegregation may be found in references [90, 91, 94, 98]. Factors controlling dendrite arm spacings and carbide sizes are discussed in references [93, 96, 97].
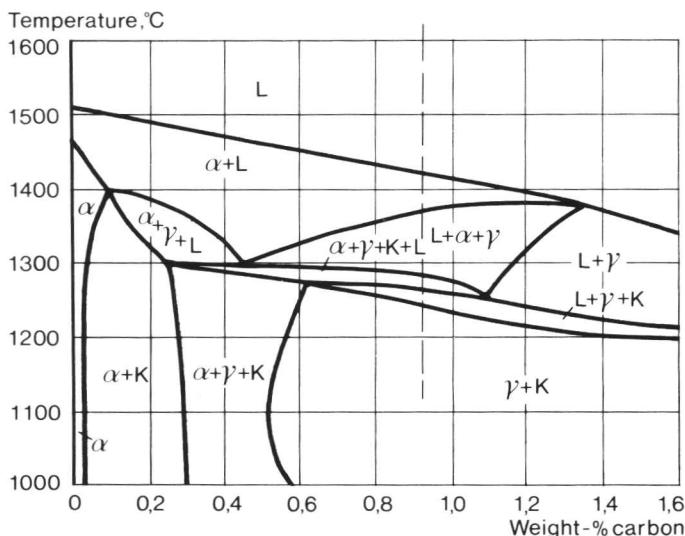
Figure 5.1 Phase diagram for steel with approx. 4% Cr, 5% Mo, 6% W and 2% V. (After Horn E. & Brandis H., *DEW-Techn. Ber.* 11 (1971), 147–154) [89]

STEEL 501. 0,9 % C 4 % Cr 5 % Mo 6 % W 2 % V HIGH SPEED STEEL

Designations

SIS	AISI	Werkstoff Nr
2722	M 2	1.3343

Composition (wt–%)

C	Si	Mn	P	S	Cr	Ni	Mo	Cu	Co	W	V	Al_{tot}	N
0,88	0,30	0,32	0,030	0,017	3,9	0,36	4,9	0,10	0,30	6,1	1,9	0,022	0,036

Thermal Analysis
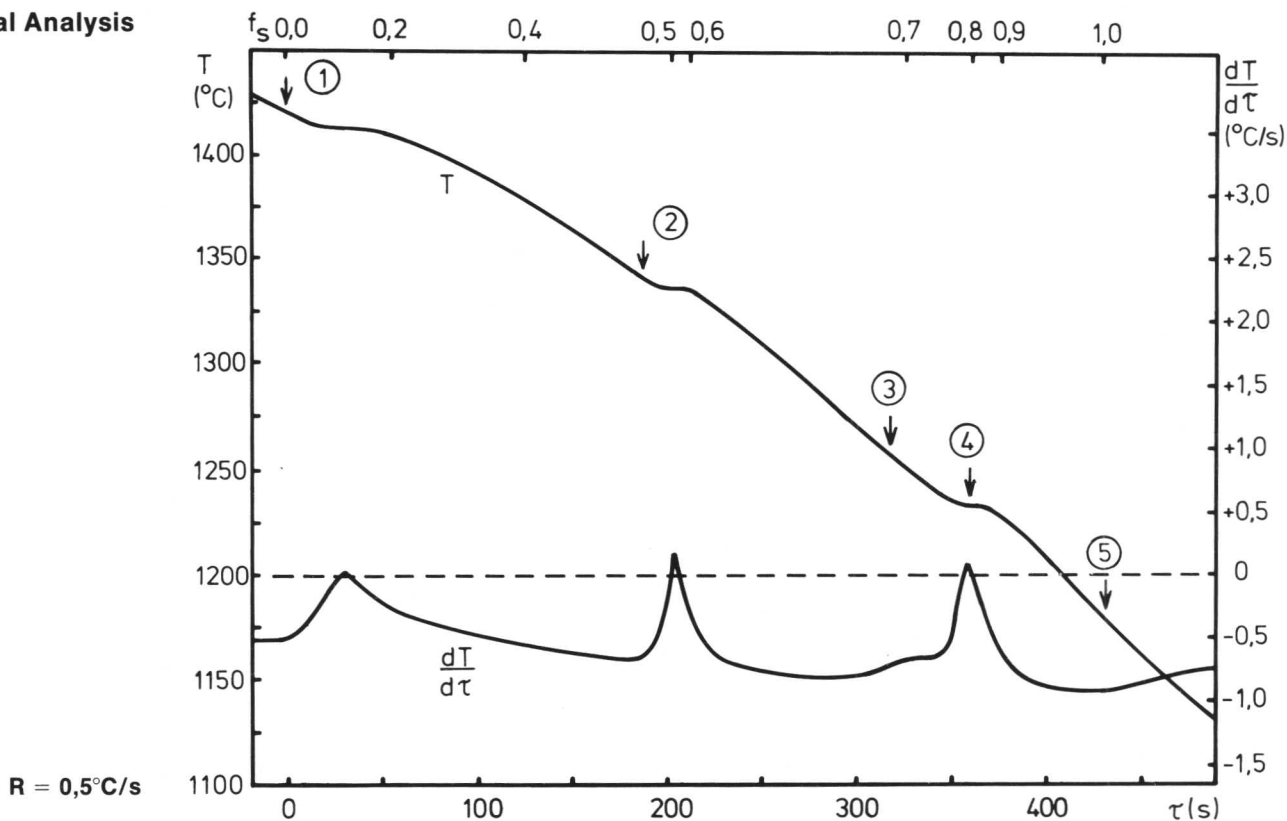
	Average Cooling Rate, R, (°C/s)		
	2,0	**0,5**	**0,1**
Liquidus temperature, ferritic primary phase, °C ①	1414	1423	1427
Temperature of start of austenite formation, °C ②	1341	1342	1350
Temperature of start of MC-austenite eutectic formation, °C ③	1260	1260	1270
Temp. of M_2C- and M_6C-austenite eutectic formation, °C ④	1228	1232	1255
Solidus temperature, °C ⑤	1175	1185	1220
Solidification range, °C	240	240	210
Solidification time, s	170	455	2500

Precipitates

MC-M_2C- and M_6C-austenite eutectic. The amount of carbide eutectic decreased with increasing cooling rate, (see figures 6–9, 11–14).

MC contained approximately 45 % V, 17 % W and 11 % Mo, and M_2C approximately 37 % W, 28 % Mo and 12 % V. M_6C contained mainly Fe, W and Mo.

Microsegregation

Element	Cr	Mo	W	V	
l	1,6	1,2	0,8	0,9	R = 0,5 °C/s Tq = 1155 °C

Figure 10

R   = 0,5°C/s
Tq   = 1335°C
Peritectic reaction. Widmanstätten austenite (γ_w) precipitated in δ during quenching.

Figure 11

R   = 0,5°C/s
Tq   = 1245°C
MC-γ eutectic. The MC carbide is the first carbide to precipitate. 0,1 vol-% MC-carbide.

× 600   25 μm
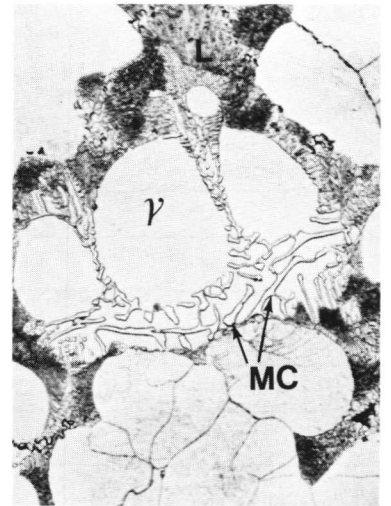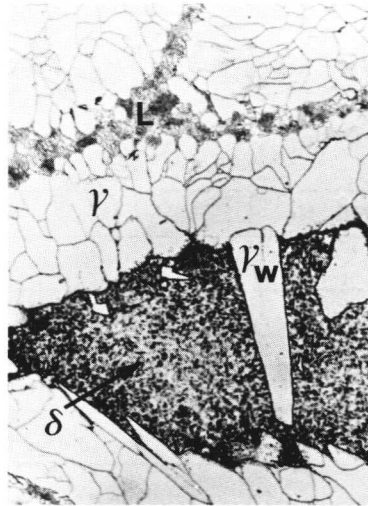
Figure 12

R   = 2,0°C/s
Tq   = 1155°C
Figures 12−14: Carbide morphologies.

× 600   25 μm

Figure 13

R   = 0,5°C/s
Tq   = 1155°C

× 600   25 μm
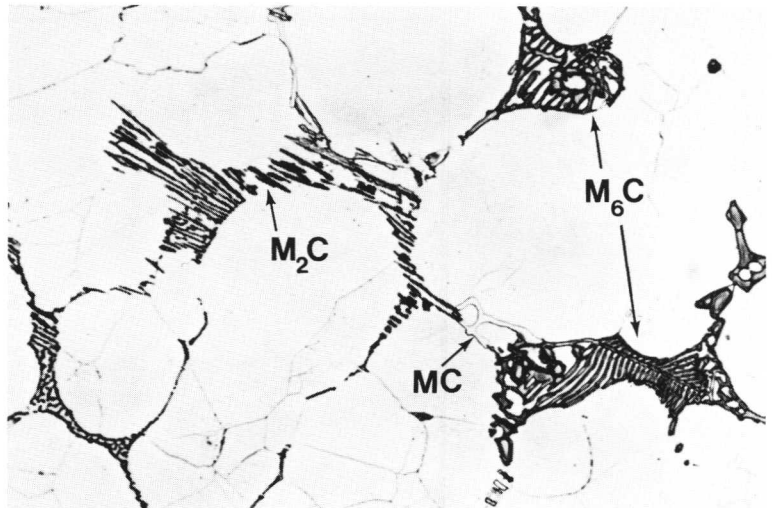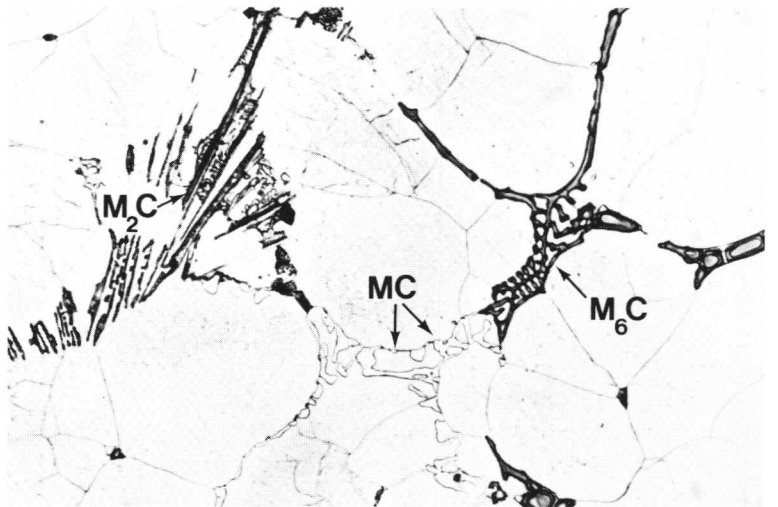
Figure 14

R   = 0,1°C/s
Tq   = 1155°C

× 600   25 μm
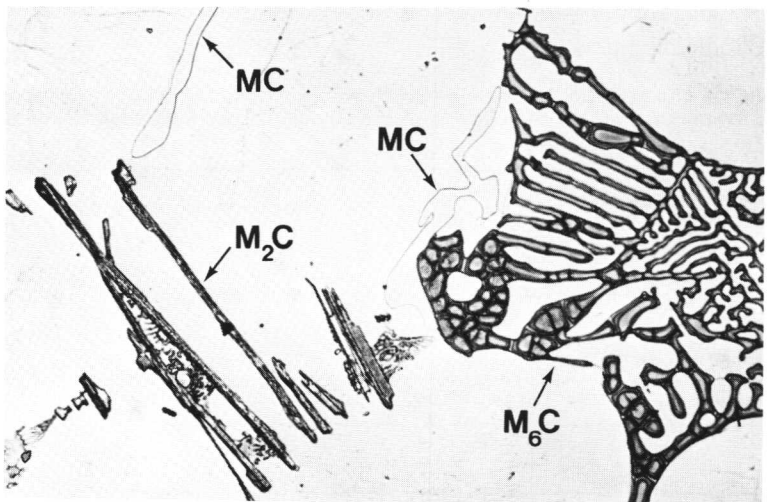
STEEL 502.   1,0 % C 4 % Cr 9 % Mo 1,5 % W 2 % V   HIGH SPEED STEEL

Designations

SIS	AISI	Werkstoff Nr
2782	M 7	1.3348

Composition (wt–%)

C	Si	Mn	P	S	Cr	Ni	Mo	Cu	Co	W	V	Al_{tot}	N
1,0	0,38	0,38	0,010	0,037	3,8	0,14	9,2	0,11	0,05	1,5	2,0	0,010	0,036

Thermal Analysis

R = 0,5°C/s
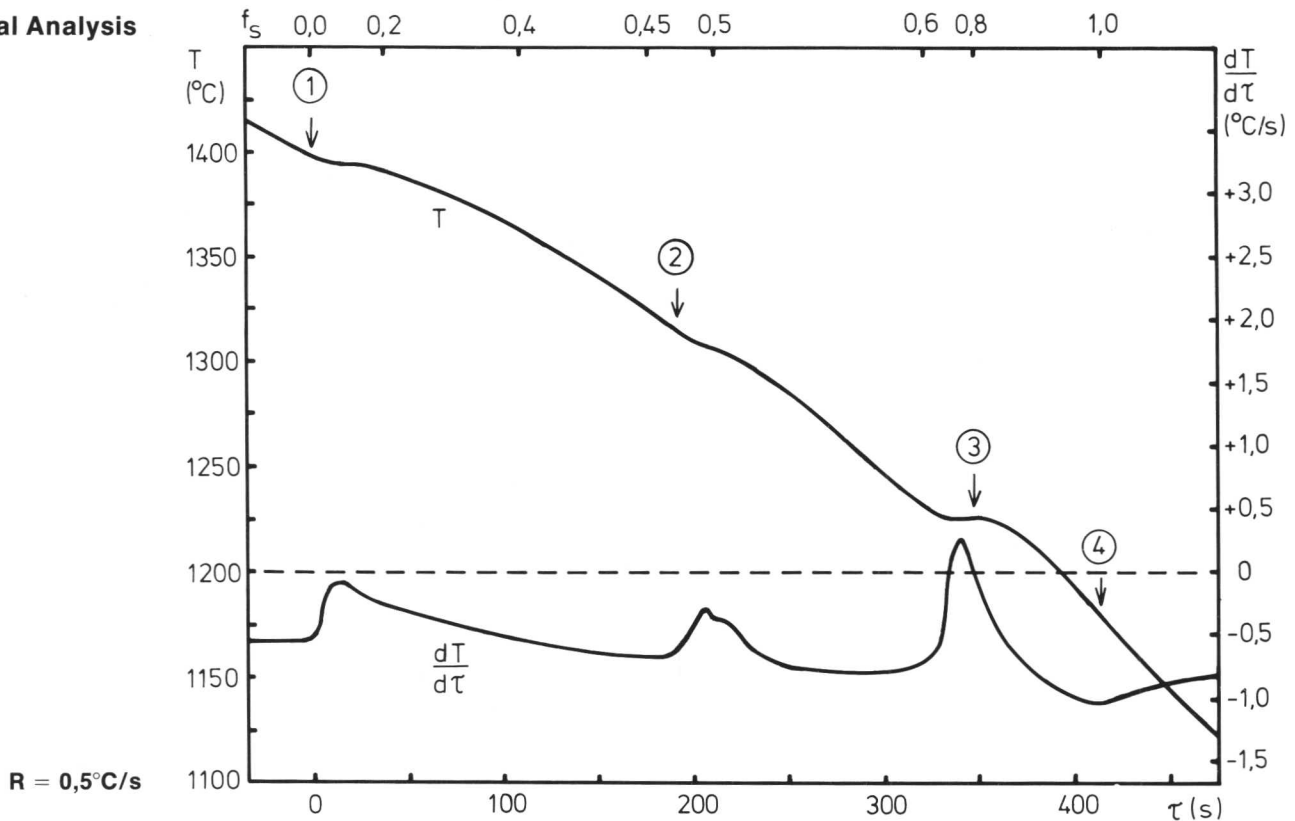
	Average Cooling Rate,R, (°C/s)		
	2,0	**0,5**	**0,1**
Liquidus temperature, ferritic primary phase, °C ①	1401	1400	1400
Temperature of start of austenite formation, °C ②	1305	1315	1322
Temperature of MC- and M_2C-austenite eutectic formation, °C ③	1222	1226	1233
Solidus temperature, °C ④	1175	1180	1185
Solidification range, °C	225	220	215
Solidification time, s	170	410	2100

The second peak on the cooling rate curve is split into two peaks, corresponding to the peritectic reaction, followed by the liquid-to-austenite transformation.

Precipitates

MC- and M_2C-austenite eutectic, (see figures 7 – 9, 12 – 14).

M_2C contained approximately 57 % Mo, 11 % V and 9 % W. MC was of the VC type.

Microsegregation

Element	Cr	Mo	W	V	
I	1,8	1,1	0,6	0,7	R = 0,5 °C/s Tq = 1155 °C

Partly solidified

Figure 1

R = 0,5°C/s
Tq = 1310°C
d = 35 μm

δ-dendrites, partly transformed to γ, and quen-
ched liquid (L), (compare figures 5 and 6).
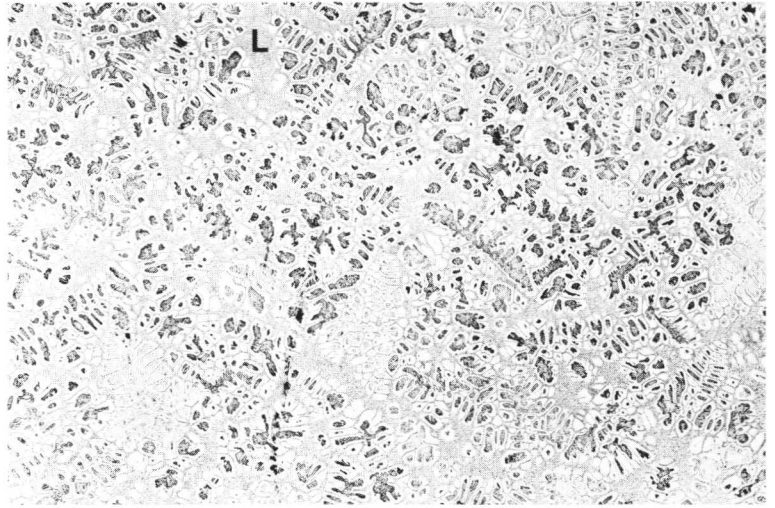
× 25   400 μm

Completely solidified

Figure 2

R = 2,0°C/s
Tq = 1155°C
d = 25 μm

Figures 2−4: γ-dendrites and carbide eutectics,
(compare figure 7).

× 25   400 μm

Figure 3

R = 0,5°C/s
Tq = 1155°C
d = 35 μm

(Compare figure 8.)
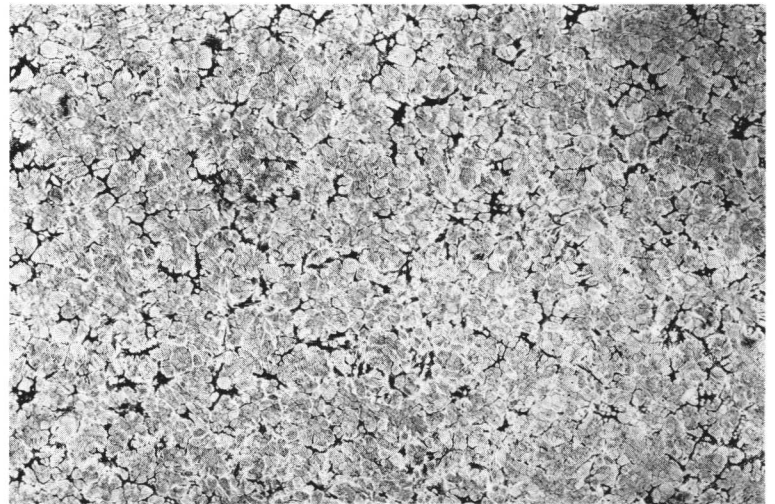
× 25   400 μm

Figure 4

R = 0,1°C/s
Tq = 1155°C
d = 70 μm

(Compare figure 9.)

× 25   400 μm
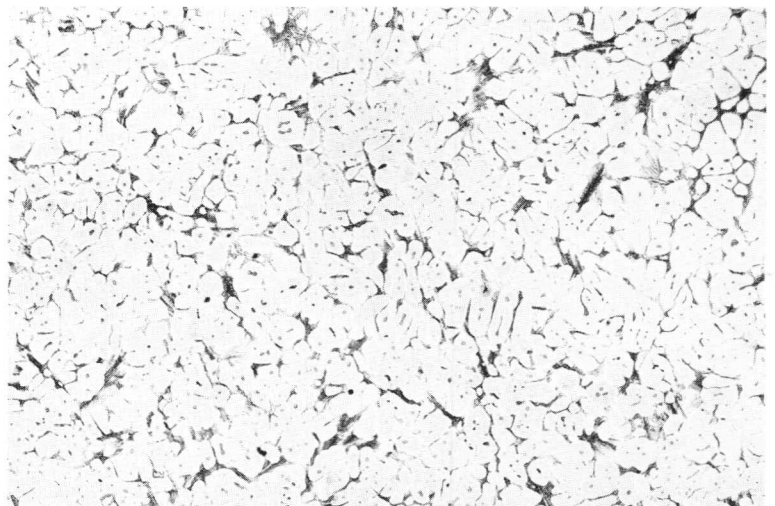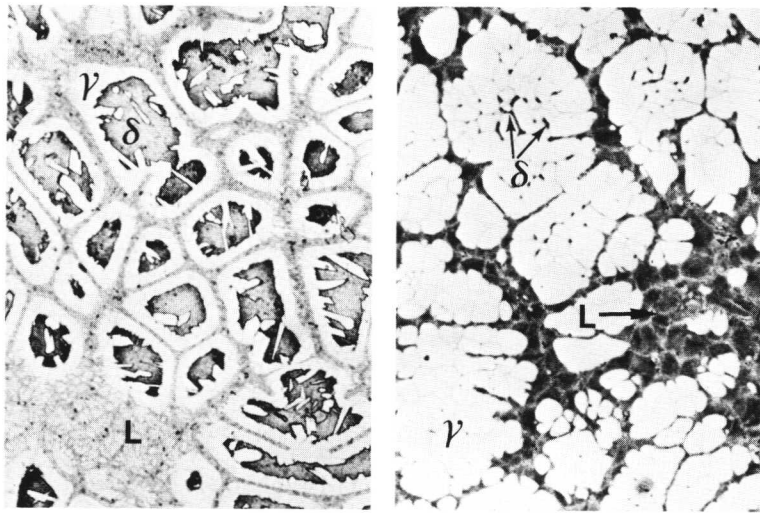
Figure 5
R = 0,5°C/s
Tq = 1310°C
Peritectic reaction and transformation,
(compare figure 10.)

Figure 6
R = 0,5°C/s
Tq = 1260°C
Growth of austenite, $\delta \rightarrow \gamma$ and $L \rightarrow \gamma$. Extensive nucleation of γ after the peritectic reaction, (see cooling curve and compare steel 501, figure 6).

100 μm × 150
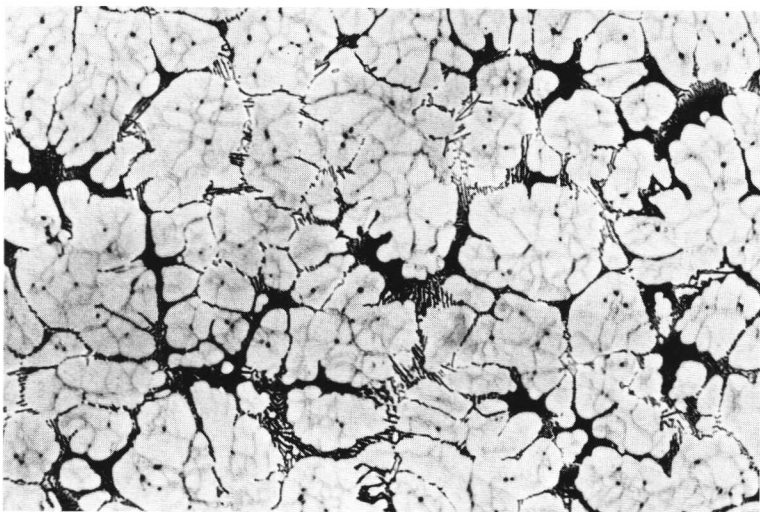
Figure 7
R = 2,0°C/s
Tq = 1155°C
Figures 7−9: Carbide structure. Note the influence of cooling rate on carbide coarseness, (compare figure 12).

100 μm × 150
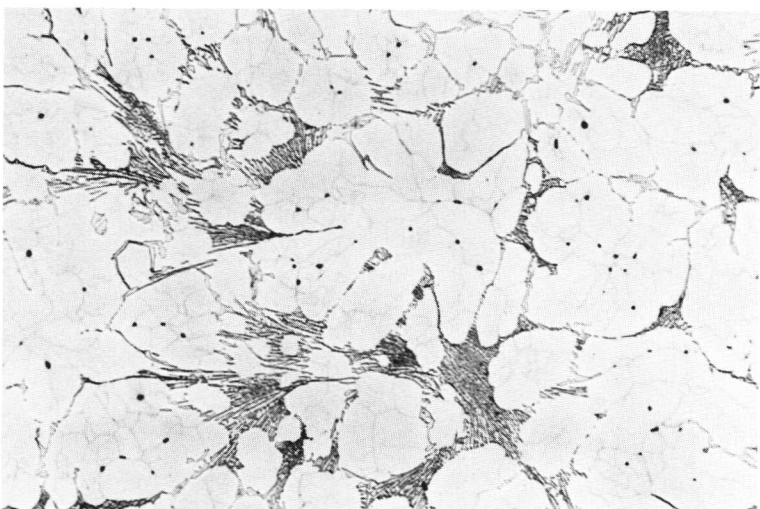
Figure 8
R = 0,5°C/s
Tq = 1155°C
9 vol-% carbides (MC and M_2C),
(compare figure 13).

100 μm × 150
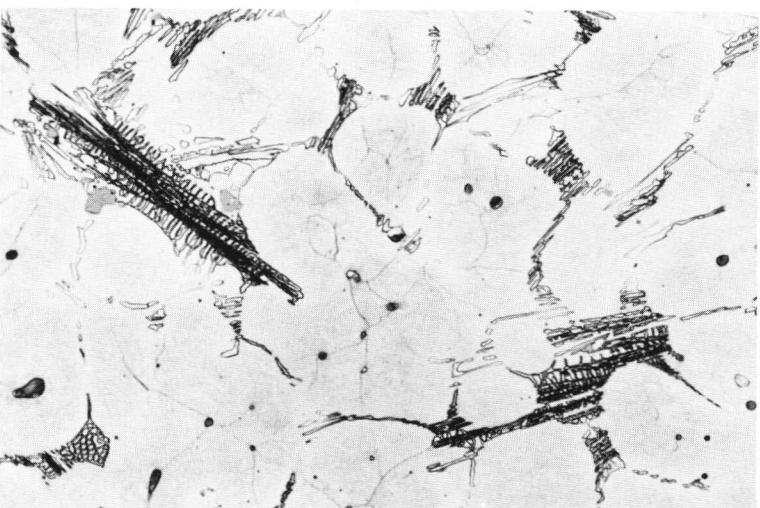
Figure 9
R = 0,1°C/s
Tq = 1155°C
10 vol-% carbides (MC and M_2C),
(compare figure 14).

100 μm × 150

Partly solidified

Figure 1
R   = 0,5°C/s
Tq = 1335°C
d   = 35 μm
δ-dendrites, partly transformed to γ, and quenched liquid (L), (compare figures 5 and 6).

× 25   400 μm
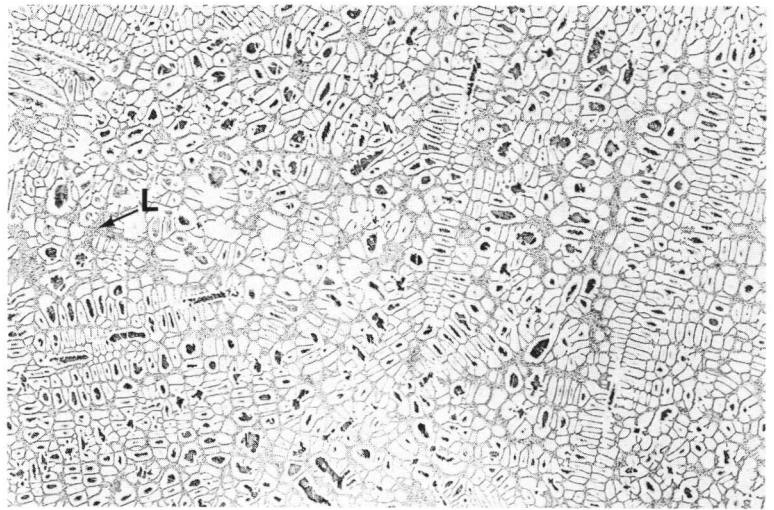
Completely solidified
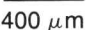
Figure 2
R   = 2,0°C/s
Tq = 1155°C
d   = 30 μm
Figures 2−4: γ-dendrites and carbide eutectics, (compare figure 7).

× 25   400 μm
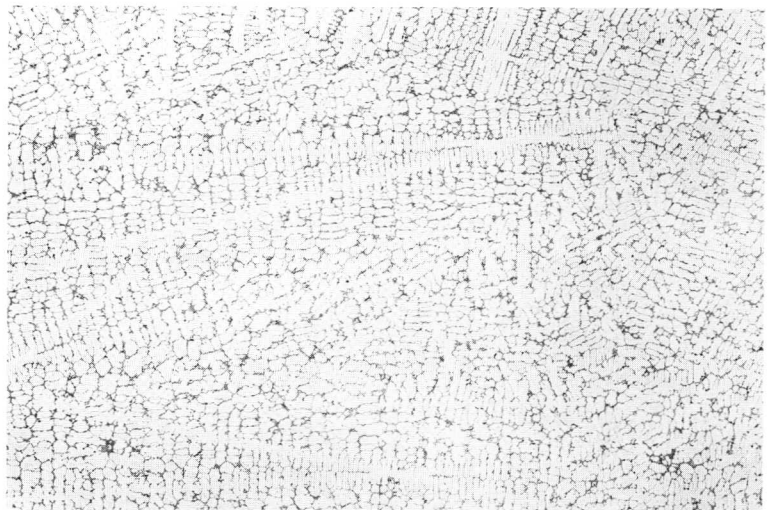
Figure 3
R   = 0,5°C/s
Tq = 1155°C
d   = 40 μm
(Compare figure 8.)

× 25   400 μm
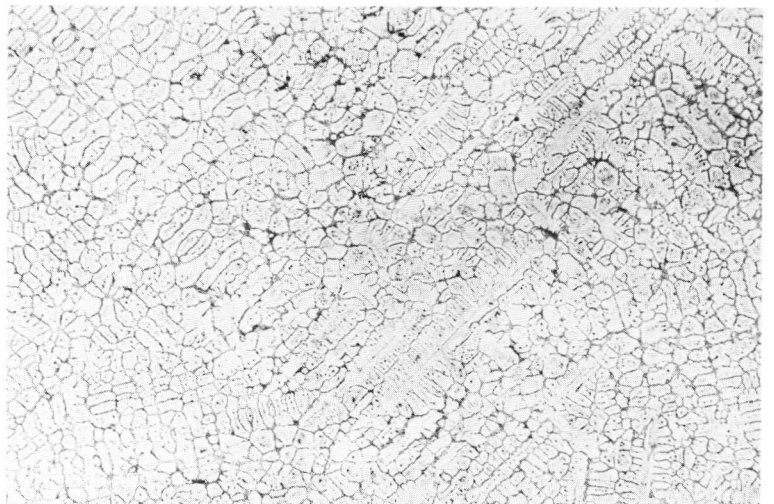
Figure 4
R   = 0,1°C/s
Tq = 1155°C
d   = 85 μm
(Compare figure 9.)

× 25   400 μm
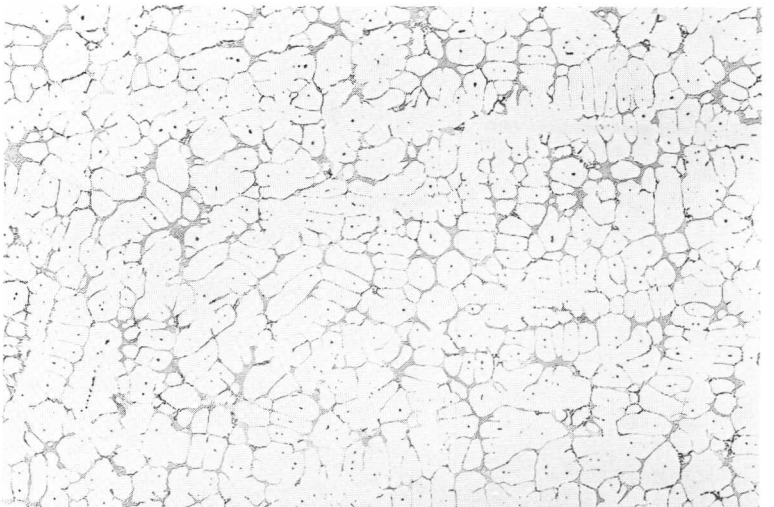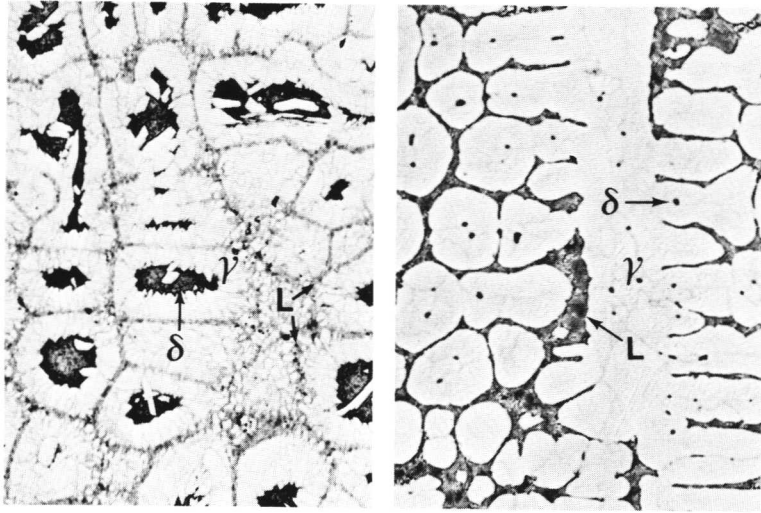
Figure 5
R   = 0,5°C/s
Tq = 1335°C
Peritectic reaction and transformation,
(compare figure 10).

Figure 6
R   = 0,5°C/s
Tq = 1245°C
Growth of austenite, $\delta \rightarrow \gamma$ and $L \rightarrow \gamma$, and MC-γ eutectic. 0,1 vol-% MC carbide,
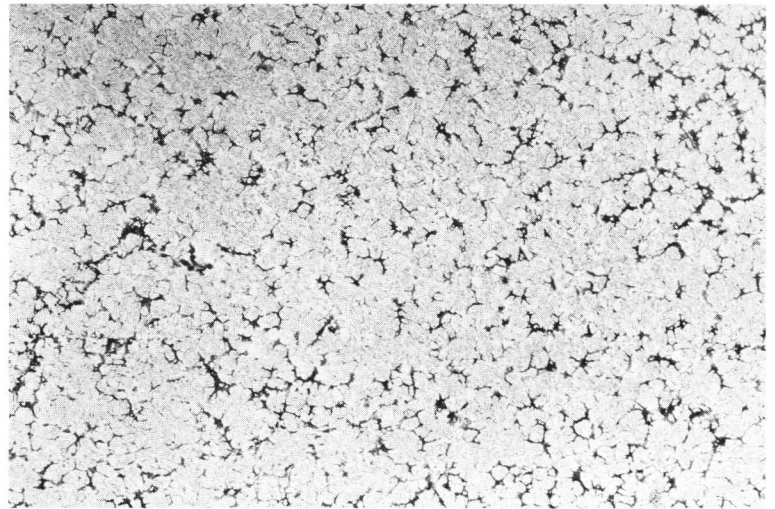(compare fig 11).

100 μm   × 150
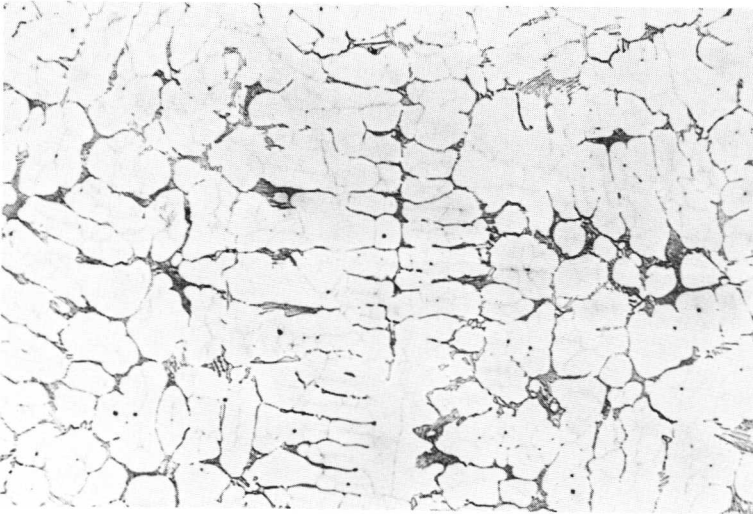
Figure 7
R   = 2,0°C/s
Tq = 1155°C
Figures 7—9: Carbide structure. Note the influence of cooling rate on carbide coarseness,
(compare figure 12).

100 μm   × 150
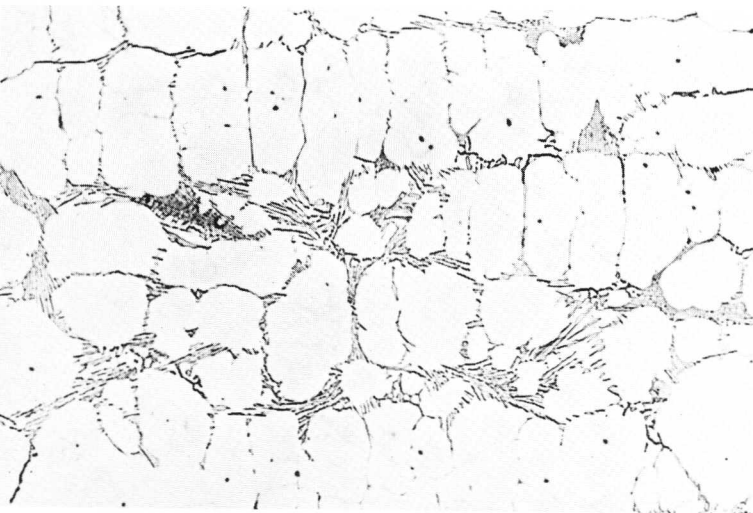
Figure 8
R   = 0,5°C/s
Tq = 1155°C
9 vol-% carbides, (MC, M_2C and M_6C),
(compare figure 13).

100 μm   × 150
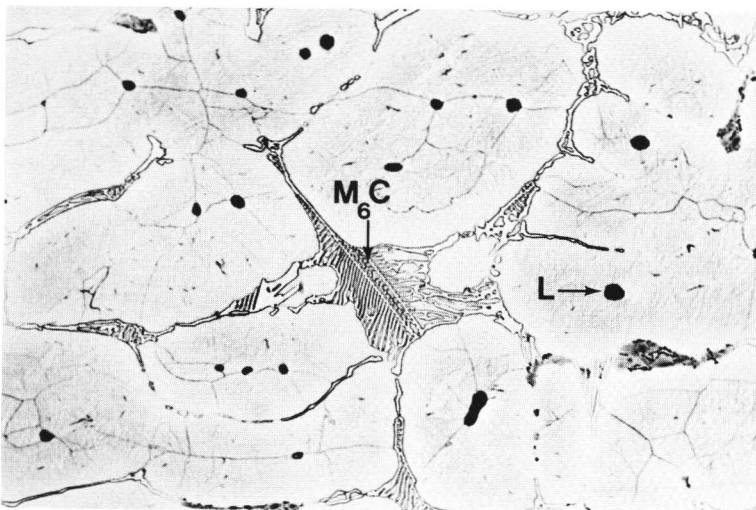
Figure 9
R   = 0,1°C/s
Tq = 1155°C
12 vol-% carbides, (MC, M_2C and M_6C),
Melted areas (L) in the centres of the dendrites.
(Compare figure 14).

100 μm   × 150

Figure 10
R = 0,5°C/s
Tq = 1310°C
δ-dendrite, surrounded by γ formed by the peritectic reaction. Widmanstätten austenite (γ_w) precipitated in δ during cooling and quenching.

× 600   25 μm
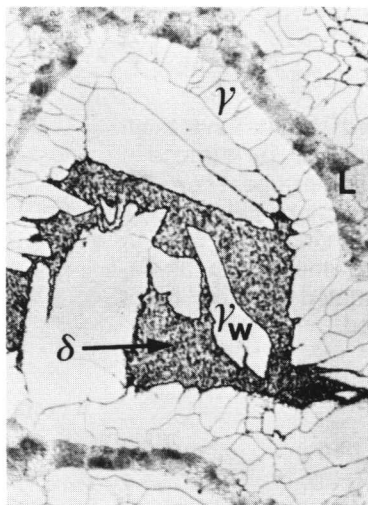
Figure 11
R = 0,5°C/s
Tq = 1260°C
γ, residual δ, and liquid (L). (No carbides.)
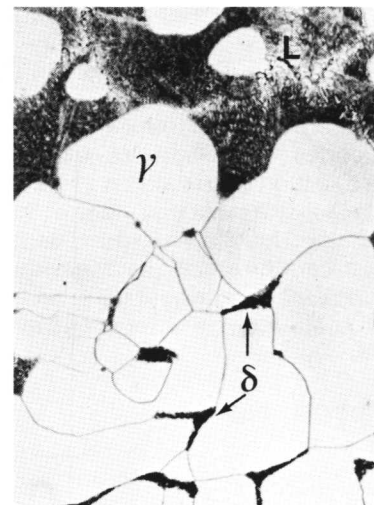
Figure 12
R = 2,0°C/s
Tq = 1155°C
Figures 12−14: Carbide morphologies.
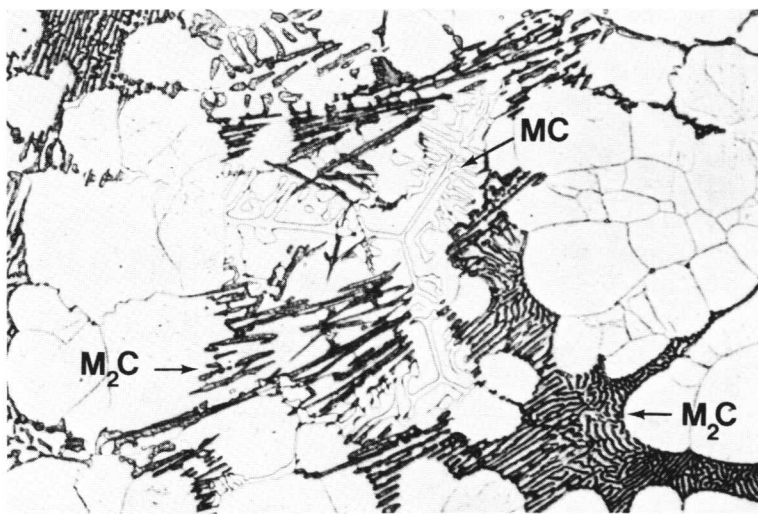
× 600   25 μm

Figure 13
R = 0,5°C/s
Tq = 1155°C
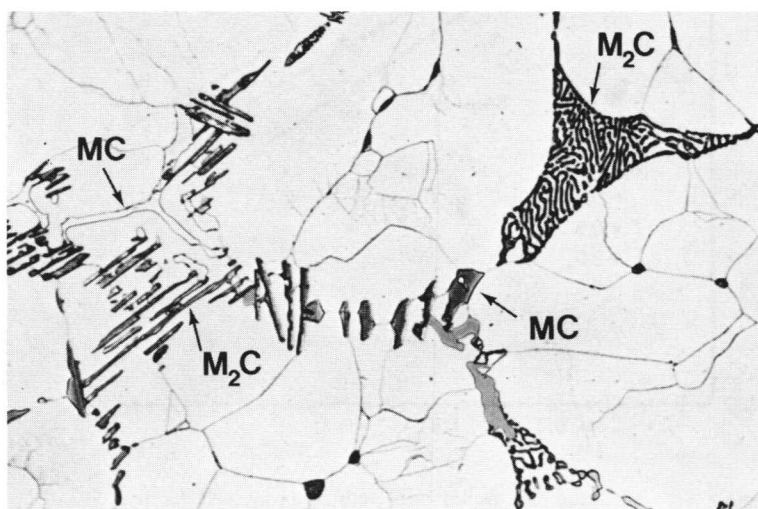
× 600   25 μm

Figure 14
R = 0,1°C/s
Tq = 1155°C
Remelted areas (L) in the centres of the dendrites.

× 600   25 μm
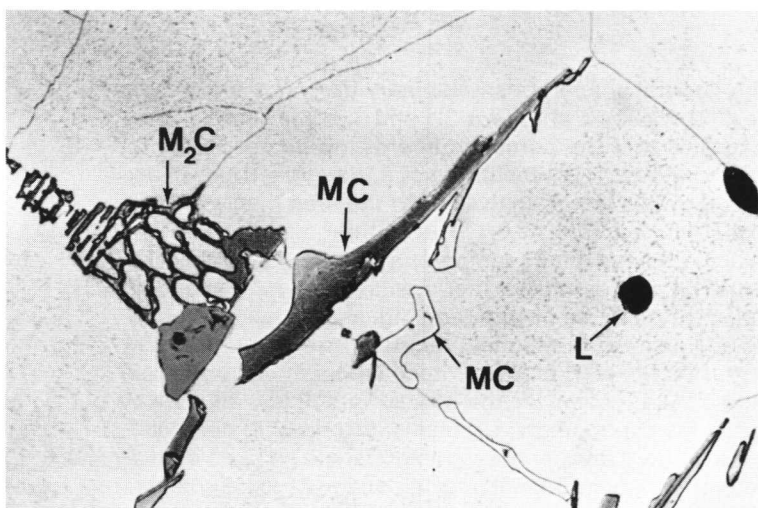
6. Conclusions and Comments

In the preceeding chapters, detailed results have been reported for individual steel compositions. The purpose of this section is to illustrate general relationships for groups of steels. The fact that many of the important solidification parameters follow a general pattern justifies interpolation between the steels the behaviour of which has been described. This allows data to be estimated for many types of steel which have not been included.

Thermal analysis

The results on liquidus, solidus and peritectic temperatures, measured for the three cooling rates, are shown as a function of the carbon content in figures 6.1−6.4 for carbon, low alloy and chromium steels. The thermal data for the stainless and heat resistant alloys are plotted as a function of alloy content, expressed as equivalents of chromium and nickel, in figure 6.6.
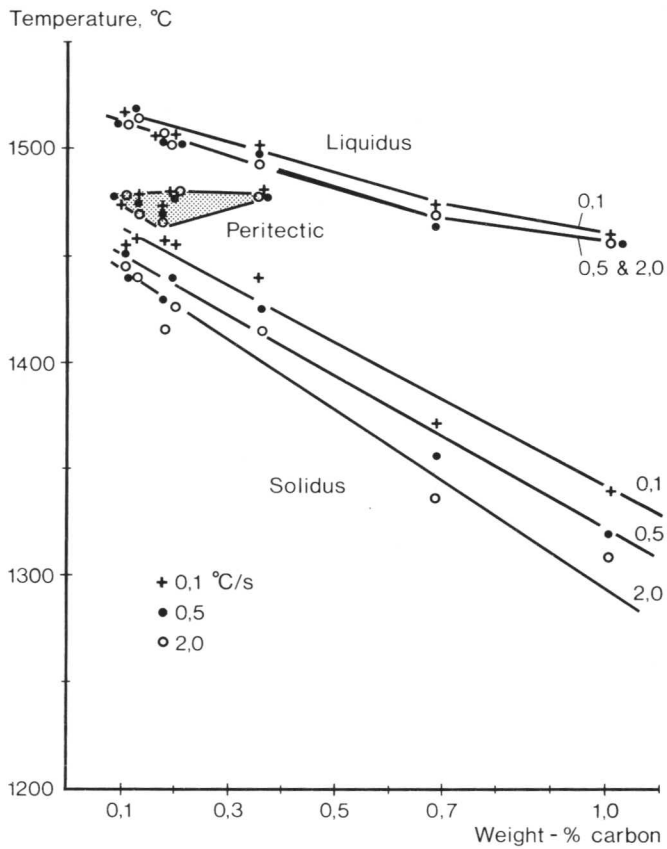
Figure 6.1 Liquidus, peritectic and solidus temperatures for carbon steels

The general shape of pseudobinary diagrams of the type Fe-C-M is shown in figures 3.1 and 3.2. It is seen in these diagrams that the peritectic line of the binary Fe-C-diagram (figure 2.1) is substituted by a triangular three-phase area, but this is not equivalent to the area marked "peritectic" in figures 6.1−6.4. The experimental points here indicate the maximum temperature of the peritectic reaction. The scatter in the experimental results depended on the varying degree of supercooling, as discussed in chapter 1. However, the highest temperatures given probably represent the start of the peritectic reaction in large scale ingots. The reason for the spread in solidus values was partly the experimental problems described in chapter 1, but also the fact that the commercial steels used contained different amounts of alloying and impurity elements.
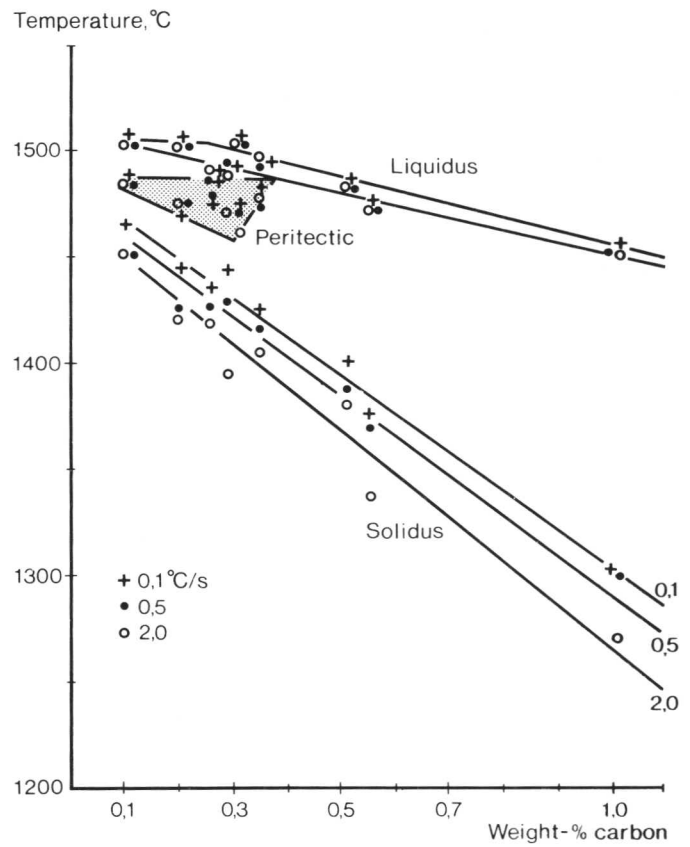
Figure 6.2 Liquidus, peritectic and solidus temperatures for low alloy steels
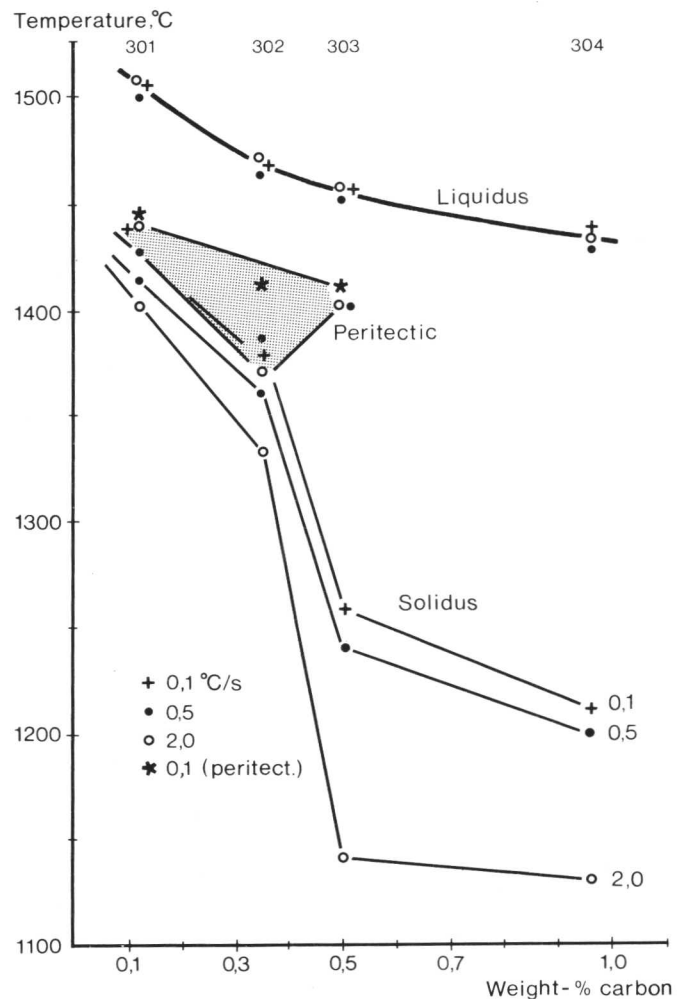
Figure 6.3 Liquidus, peritectic and solidus temperatures for 5% chromium steels
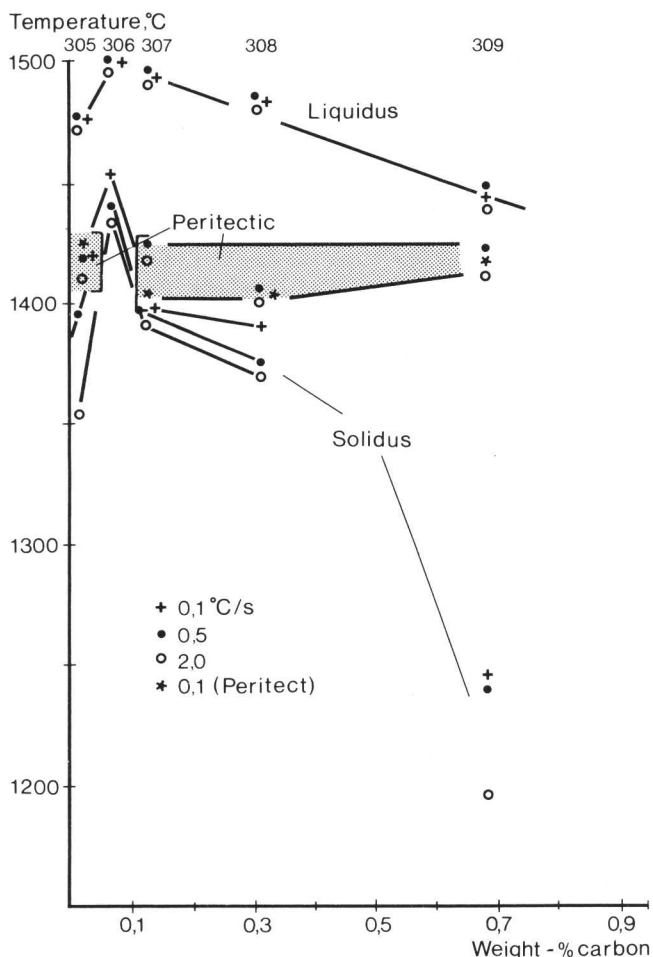
Figure 6.4 Liquidus, peritectic and solidus temperatures for 13% chromium steels

As shown in figures 6.3 and 6.4, steels 303, 304 and 309 had very low solidus temperatures explained by eutectic carbide precipitation. The pseudobinary equilibrium phase diagrams for Fe − 5Cr − C and Fe − 13Cr − C, figures 3.1 and 3.2, indicate a eutectic reaction for carbon contents of 1,2 and 0,8 % respectively. The appearance of carbide eutectics at much lower carbon concentrations is a result of microsegregation. In figure 6.4 the solidus lines have been interrupted between steels 308 and 309, as it is certain that eutectic precipitation of carbides will take place in steels with carbon contents lower than that of steel number 309.

The solidification range widened with an increasing rate of cooling, see figure 6.5. The constitutional influence of high carbon and chromium contents was very strong.

The tendency was for the liquidus and the peritectic temperatures to be independent of cooling rate, whereas the solidus was markedly lower at a higher cooling rate. The reason for this is the higher degree of backdiffusion and homogenization possible at a low cooling rate.

The main difference between the carbon and low alloy steels, shown in figures 6.1 and 6.2, was the lowering of the solidus lines by alloying elements. The liquidus temperatures were also decreased somewhat. It has not been possible to calculate the factors for the temperature depression by, for example, nickel and chromium, as the levels of other elements were not held constant in the present work. However, at the low contents present, the influence of minor changes in composition can be estimated from the binary phase diagrams.

In figure 6.4, the abnormal behaviour shown by steel number 305, containing 0,04% C, 13% Cr, 5,5% Ni, reflects the depression of both liquidus and solidus temperatures by nickel. At the 13% Cr- level the mean effect was roughly 5 and 10 degrees per weight percent of nickel for the liquidus and solidus respectively. In spite of the very low carbon content, steel number 305 had a peritectic reaction. This is an effect of nickel, as steel number 306 with a higher carbon content solidified completely to ferrite.

Figure 6.5 Solidification ranges for carbon, low alloy and chromium steels as function of cooling rate

Liquidus and solidus temperatures of the stainless and heat resistant steels are shown in figure 6.6, as a function of alloy content, expressed as equivalents of chromium and nickel as follows, [78, 83]:

$Cr_{eq} = Cr + 1.37Mo + 1.5Si + 2Nb + 3Ti$

$Ni_{eq} = Ni + 0.31Mn + 22C + 14.2N + 1Cu$

(The elements are expressed in weight percentages.)
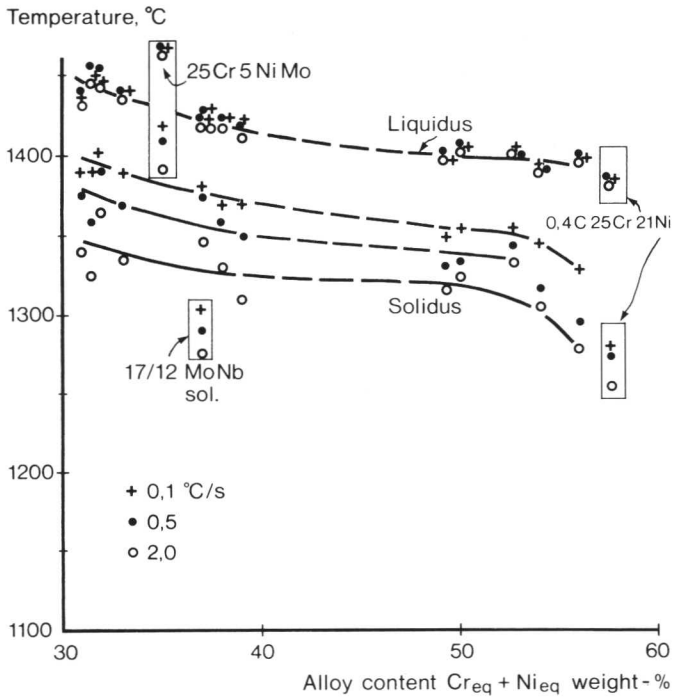
Figure 6.6 Liquidus and solidus temperatures for stainless and heat resistant steels

Again, the highest cooling rate led to the lowest solidus temperature and the widest solidification range. These ranges were comparatively narrow for this group of steels, in most cases 100°C or less (compare figure 6.5).

Two of the alloys, numbers 401 with 25% Cr, 5% Ni, 1% Mo, and 406 with 17% Cr, 12% Ni, Mo-Nb, did not follow the general trend. The ferritic alloy, 401, exhibited the highest liquidus and solidus temperatures of all the stainless and heat resistant steels examined; a constitutional effect in full agreement with the Fe-Cr-Ni equilibrium phase diagram in figure 4.1. This diagram also indicates a narrow solidification range for this composition. Alloy 406 showed very low solidus temperatures and a wide solidification range, 120–150°C. The reason was the pronounced interdendritic segregation of, mainly, niobium and carbon.

The effect of carbon can be seen in alloy 414, with 25% Cr, 21% Ni, 0,4% C. This had a solidification range of 105–125°C, and very low solidus temperatures as a result of interdendritic segregation.

From the thermal analysis data for the stainless and heat resistant steels, the fraction solidified primarily as δ-ferrite was evaluated. The results are given in figure 6.7 as a function of the ratio between the chromium and nickel equivalents, as defined above. It may be seen that a drastic change in solidification behaviour takes place between Cr and Ni equivalent ratio values of 1,35 and 1,80; alloys with values below this range solidify as 100% austenite, above this range as 100% ferrite. Behaviour of this kind may also be seen in figure 4.1. No substantial influence of cooling rate on the fraction of δ-ferrite formed was observed.

The two high speed steels, (numbers 501 and 502), had solidification ranges wider than 200°C, which is in good agreement with their high concentration of carbon and alloying elements. The highest cooling rate corresponded to the lowest solidus temperature and the widest solidification range, as for the other alloy systems in this work, (see figure 6.5).
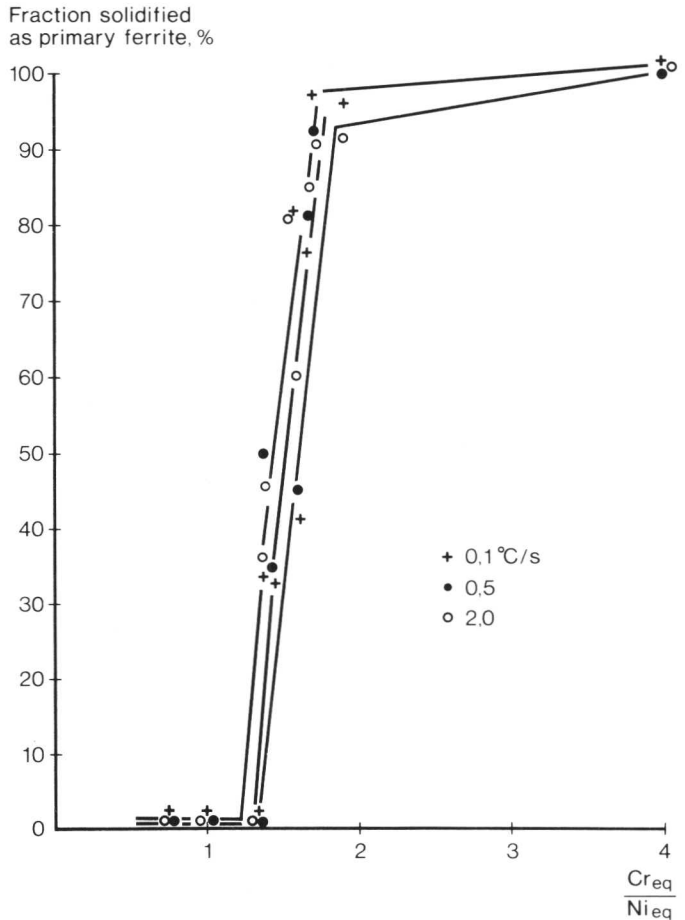
Figure 6.7 Fraction solidified as δ-ferrite in stainless steels

Microsegregation

The microprobe results were derived from samples cooled at 0,5°C/s and quenched from just below the solidus temperature. The dependence on carbon level of the microsegregation of manganese and chromium in carbon, low alloy and chromium steels is shown in figures 6.8 and 6.9.

The high values of the segregation ratio I found at high carbon levels were caused by slow backdiffusion in austenite, and by a negative interaction known to exist at least between carbon and chromium, [31, 47]. Primary formation of austenite was noted at a carbon content above some 0,4% in carbon and low alloy steels, (chapter 2), whereas no chromium steel solidified by formation of primary austenite, (chapter 3). As shown in figure 6.9, the chromium steel number 306, with 0,07% C and 13% Cr, which solidified completely as ferrite, had no measurable chromium segregation; emphasizing the importance of diffusion in ferrite during solidification in reducing the observed segregation. In contrast, steel number 305, with 0,04% C, 13% Cr, 5,5% Ni, solidified partly to austenite and showed chromium segregation, despite having a lower carbon content. Molybdenum, which was present in appreciable amounts in all the 5% chromium steels, displayed the same segregation behaviour as chromium in relation to carbon, figure 6.10.
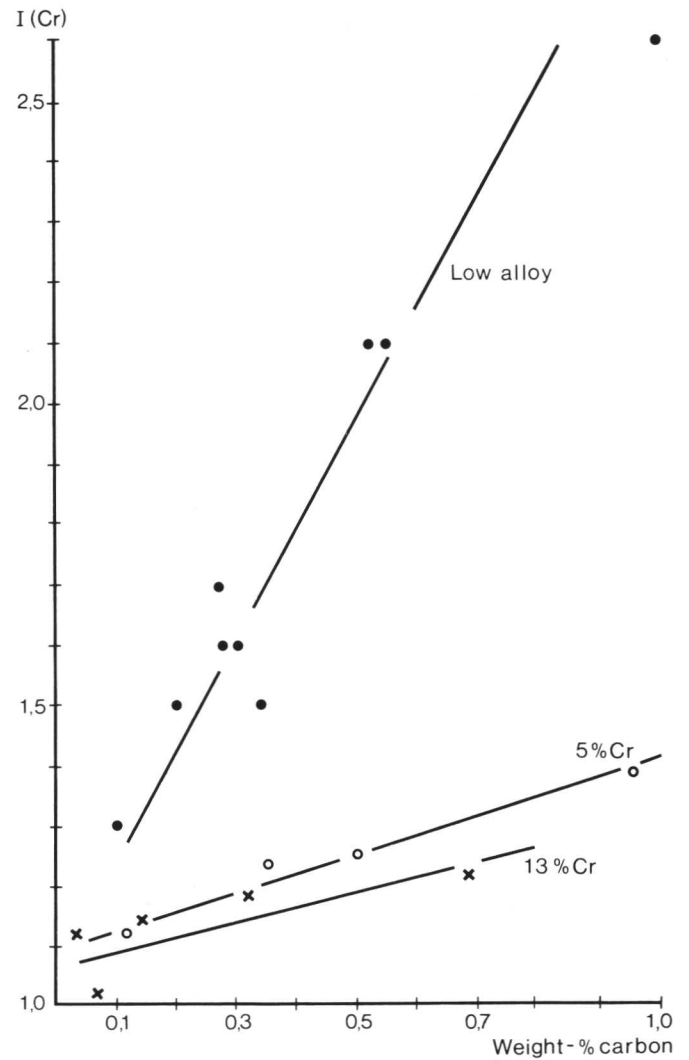
Figure 6.9 Microsegregation of chromium in low alloy and chromium steels
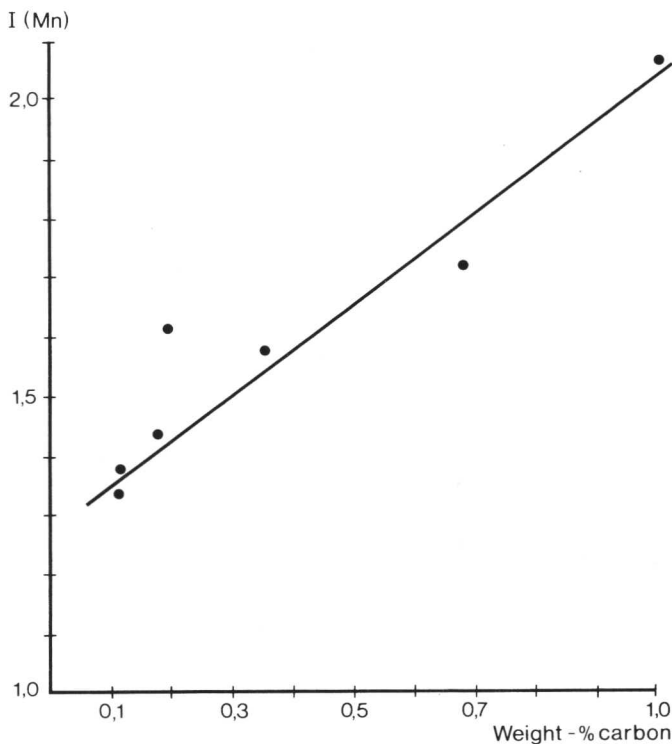
Figure 6.8 Microsegregation of manganese in carbon steels
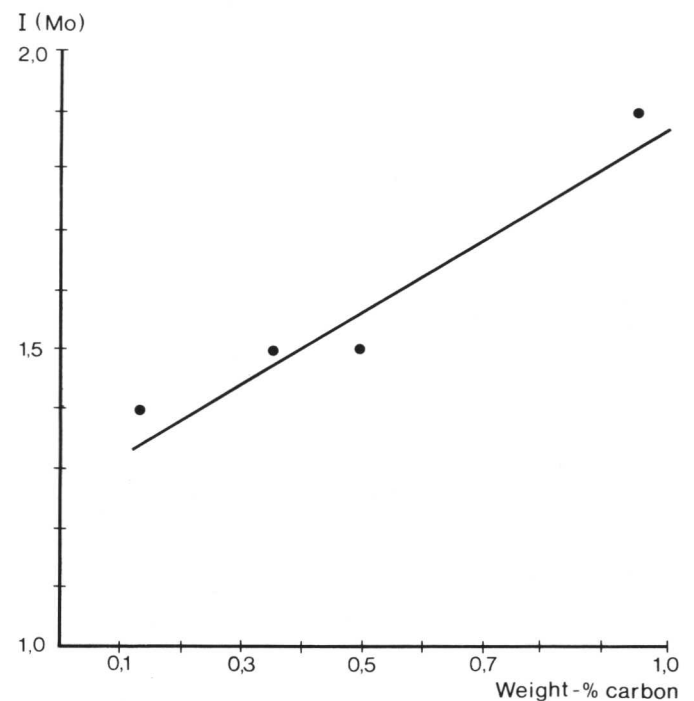
Figure 6.10 Microsegregation of molybdenum in 5% chromium steels

As shown by comparison between figures 6.9 and 6.11, nickel segregated less than chromium in the low alloy steels, the segregation ratio for the element having an inverse relationship with carbon.

The segregation ratio, I, and partition ratios of chromium and nickel in the stainless and heat resistant steels are shown in figures 6.12 and 6.13. These ratios were defined in chapter 1 as follows:

$$I = \frac{C_{x,\,ID}}{C_{x,\,D}}$$

$$P_D = \frac{C_{x,\delta_D}}{C_{x,\gamma_D}}$$

$$P_{ID} = \frac{C_{x,\delta_{ID}}}{C_{x,\gamma_{ID}}}$$

where D and ID represent dendrites and interdendritic areas; C_x is the mean value of the concentration in these regions.

The chromium-nickel equivalent ratio decreases from left to right in figures 6.12 and 6.13. The corresponding alloy compositions are given in table 4.2.

In a steel solidifying completely as ferrite, number 401, chromium did not segregate at all but nickel did. When both austenite and ferrite were formed, in steels such as numbers 402–406, strong nickel segregation was observed together with slight, hardly measurable segregation of chromium. In the fully austenitic mode of solidification, numbers 409–415, chromium and nickel both segregated moderately. Steels 407 and 408, which formed the smallest amount of primary ferrite, were similar to the fully austenitic steels in regard to microsegregation of chromium and nickel.

The interpretation of these results is that, in the austenitic mode of solidification, both chromium and nickel segregate to the interdendritic liquid, whereas only nickel segregates in the ferritic mode. The high I (Ni)-values in the ferritic-austenitic steels are remarkable.

Figure 6.11 Microsegregation of nickel in low alloy steels
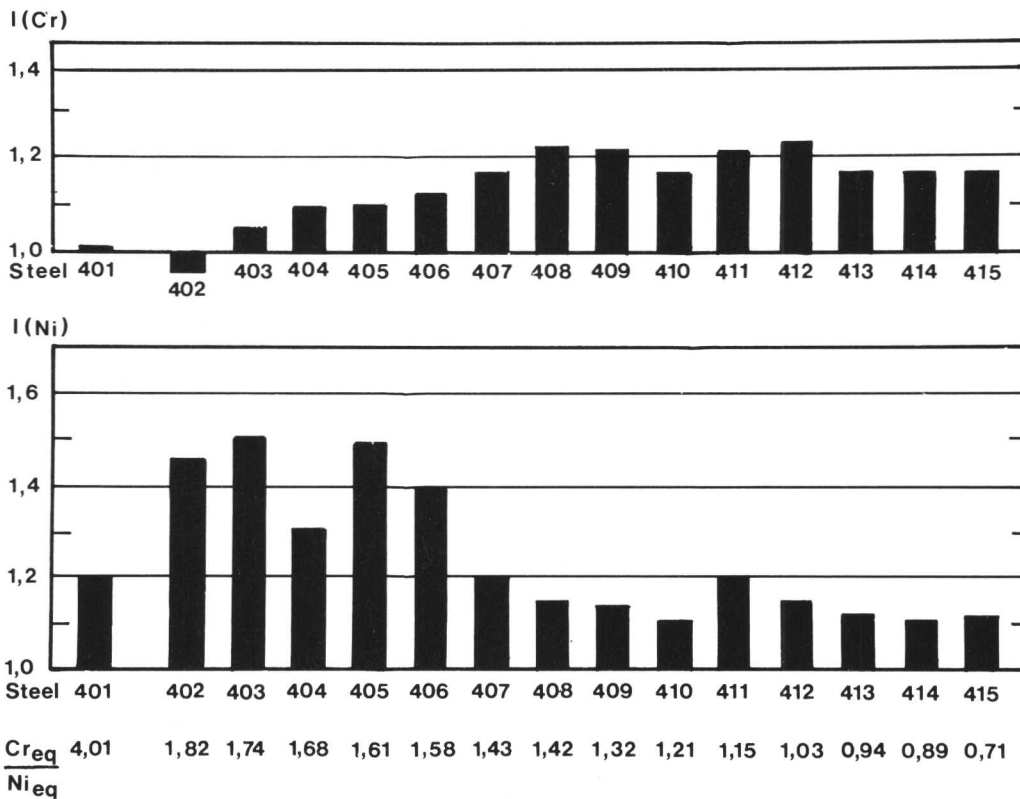
Figure 6.12 Microsegregation of chromium and nickel in stainless and heat resistant steels

The segregation of silicon, manganese and molybdenum in stainless and heat resistant steels is shown in figures 6.14 a and b. The interdendritic areas were enriched by all these elements and the interdendritic segregation of both manganese and silicon was higher in the fully austenitic, as compared to the ferritic-austenitic solidification mode. On changing from a fully ferritic solidification path, as in steel 401, to one producing a fully austenitic structure, the intensity of molybdenum (and manganese) segregation increased markedly.

Titanium in steel number 405 was found both in the inter-dendritic austenite and in the carbides. Niobium in steel 406 segregated to the interdendritic ferrite and was also present as carbides. In steel 413, the interdendritic areas were enriched with copper.

In high speed steels, the segregation measurements on the alloying elements showed that these were present mainly as constituents of carbide phases. It should be noted that the amount of eutectic carbides decreased with increasing cooling rate. The reverse behaviour was found for the austenitic steel number 414, with 0,4 % C, 25 % Cr, 21 % Ni and steel number 309, with 0,7 % C, 13 % Cr. The eutectic carbide content of these steels rose as the cooling rate was increased. The observed phenomena are in full agreement with earlier reports, [62, 63, 94]. Finally, when following the details of the solidification of the two high speed steels, it will be seen that they differed in regard to the types of carbides precipitated.

Figure 6.13 Partition ratios for chromium and nickel in stainless and heat resistant steels.

Strictly, the segregation ratio I should only be determined in a truly single phase structure, which was not the case for most of the stainless steels studied. The partition ratio P_D, between ferrite and austenite due to the peritectic reaction and the solid phase transformation of the dendrites, is shown in figure 6.13 for steels 402−406, which formed the most ferrite on solidification. From number 406 onwards the primary ferrite was gradually substituted by austenite as the primary phase, until from number 409 onwards austenite was the only primary phase, see figure 6.7. However, as chromium and other ferrite-forming elements such as molybdenum, niobium and silicon segregate from the growing austenitic phase, ferrite can form interdendritically. When the fraction of austenite-forming elements in the steel increases, the amount of interdendritic ferrite decreases. The content of interdendritic ferrite, first seen in significant amounts in steel number 406, thus passed through a maximum on going from a ferritic to an austenitic solidification path. The partition ratio P_{ID}, between the interdendritic ferrite and austenite, is shown for steels 406−410. The P-values show the enrichment of chromium in ferrite and that of nickel in austenite.

Figure 6.14 b Segregation of manganese and molybdenum in stainless and heat resistant steels.

Ferrite in stainless steels

As discussed in the preceeding paragraph, the δ-ferrite in the solidification structure of stainless steels may be of either or both dendritic or interdendritic forms. The dendritic ferrite formed as a primary phase is not enriched in solute elements, unlike the interdendritic δ-ferrite, which forms as a result of segregation. The latter type was usually seen to be larger in size than the residual, dendritic δ-ferrite. As a consequence of this difference in size and degree of segregation, the non-equilibrium dendritic ferrite will in most cases disappear more quickly than the interdendritic form during homogenizing heat treatments.

Ferrite contents were obtained by both magnetic measure-ments and optical examination. The average ferrite

There was some scatter in the ferrite measurements and the data fell into two groups with no steels in the region between the two populations. However, the measure-ments can be interpreted in terms of the solidification behaviour. Figure 6.15 shows that the ferrite content at the solidus was not influenced by cooling rate, but was governed by the composition. It was shown previously, in figure 6.7, that no primary ferrite is formed when the Cr-Ni equivalent ratio is less than 1,35. The two populations shown in figures 6.15 and 6.16 therefore represent steels forming predominantly interdendritic and dendritic ferrite respectively. For a given homogenization time the steels with mainly dendritic ferrite, which solidify with a higher
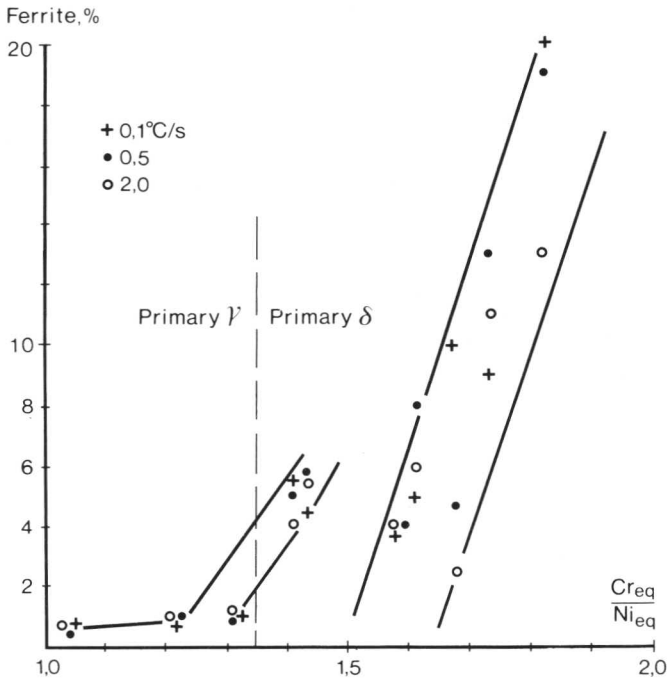
Ferrite,%

Figure 6.15 δ-ferrite in stainless steels at the solidus.

These findings can be used to explain the observation that the surface regions of stainless steel ingots, or continuously cast billets and slabs, have a lower ferrite content than the central regions. As described above, there is no effect of cooling rate on ferrite content at the solidus. However, the faster cooling rate at the surface, compared to the centre, produces a finer dendrite arm spacing. The resultant fine structure is more rapidly homogenized on cooling below the solidus.
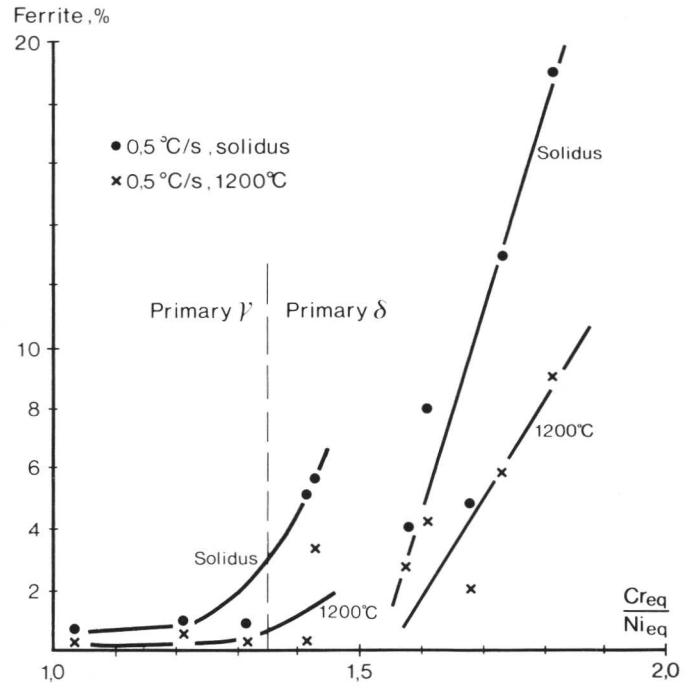
Ferrite,%

Figure 6.16 δ-ferrite in stainless steels at the solidus and 1200°C.

tic to dendritic forms of ferrite which explains the higher ferrite contents shown in figures 6.15 and 6.16 for steels of Cr-Ni equivalent ratio of about 1,4, compared to those at about 1,6. This is further supported by the amount of interdendritic ferrite probably reaching a maximum at equivalent ratios of about 1,4.

Secondary dendrite arm spacing, μm

1 ○ Carbon steels
2 ✕ Low alloy steels
3 △ 5% Cr-steels
4 • Stainless & heat resistant steels No.406-415
5 ⊙ High speed steels
○ Mean value

Secondary dendrite arm spacings

A summary of the results is presented in figures 6.17 and 6.18. In figure 6.17 the effect of cooling rate and alloy content can be seen. It is accepted that the arm spacing decreases when the alloy content increases, although a linear relationship has not been detected. The results for 13% Cr-steels and the stainless steels numbers 401–405 are not presented in figure 6.17 because of the difficulties in measuring arm spacings accurately. The dendrites were poorly defined because of the high degree of homogenization occurring in these steels during solidification.

For the 13% Cr-steels it was seen that the dendrite arm spacings decreased when the carbon content increased, and there was also a tendency in this direction for other groups of steels. This would partly account for the large spread between individual points in figure 6.17.

The well known coarsening process which occurs during solidification may be seen by comparing values at 0,5°C/s obtained in samples partly and completely solidified, figure 6.18. The final arm spacings of the dendrites are determined by the local solidification time, which here is roughly the reciprocal of the cooling rate. The results are accordingly in agreement with previously reported data, see for example figure 1.2.
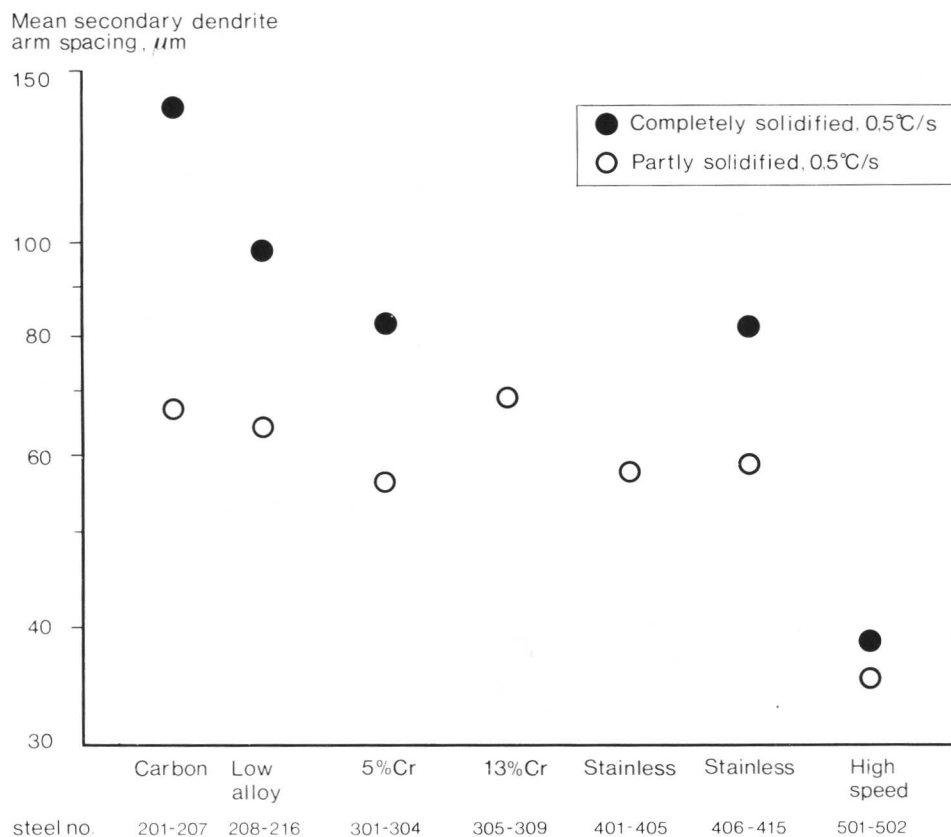
Figure 6.18 Dendrite arm coarsening during solidification

7. References

Experimental techniques and general

1. Jonsson K. O., Solidification studies with radioactive isotopes and thermocouples. *Jernkont. Ann.*, 153 (1969), 193–199

2. Chuang Y. K. & Schwerdtfeger K., Erstarrungsgeschwindigkeit von Eisen-Kohlenstoff Legierungen mit 0.6 bis 1.85% C beim Brammenguss. *Z. Metallkunde*, 64 (1973) 672–677

3. Jacobi H., Einfluss der δ-γ-Umwandlung des Eisens auf den Wärmeübergang zwischen Block und wassergekühlter Kupferkokille. *Arch. Eisenhüttenwes.*, 47 (1976), 6, 345–350

4. Lepie G. & Rellermeyer H., Untersuchungen über den Erstarrungsverlauf in Gussblöcken. *Arch. Eisenhüttenwes.*, 37 (1966) 12, 925–934

5. Mizikar E. A., Mathematical heat transfer model for solidification of continuously cast steel slabs. *Trans. AIME*, 239 (1967) 1747–1753

6. Baumann H. G., Temperaturprofile gegossener Stahlstränge. *Stahl u. Eisen*, 89 (1969) 26, 1467–1473

7. Thomas J. D. & Tzavaras A. A., Solidification and solidification rates in continuous casting of steel. *Proceedings of the Continuous Casting Symposium of the 102 AIME annual meeting, Metallurgical Society of AIME*, 1973, 125–140

8. Holzgruber W. & Tarmann B., Secondary cooling in continuous casting and it's influence on solidification parameters. *Steel Times*, 195 (1967) 217–225

9. Petrov A. K. et al, Solidification of metal powders during the atomization of a liquid phase. *Sov. Powder Metall. Met. Ceram.* 12 (1973) 1, 13–16

10. Dorschu K. E., Control of cooling rates in steel weld metal. *Weld. J., Res. Suppl.*, 47 (1968) 49 s–62 s

11. Schulze G. & Krafka H., Untersuchungen über den Einfluss von Erwärm- und Abkühlgeschwindigkeit auf das Zähigkeitsverhalten unlegierter und niedriglegierter Stähle. *Schweissen u. Schneiden*, 29 (1977) 5, 179–183

12. Ericson L. & Fridfeldt C., *Thesis Royal Institute of Technology, Stockholm, 1970*

13. Larén I. & Fredriksson H., Relations between ingot size and microsegregation. *Scand. J. Metallurgy.* 1 (1972) 59–68

14. Bäckerud L. & Edvardsson T., Influence of process variables during submerged arc welding on the primary structure, *Scand. J. Metallurgy*, 4 (1975) 267–272

15. Modin H. & Modin S., Metallurgical microscopy. *Butterworths*, London (1973)

16. Wlodawer R., Die technologische Kalorimetrie. *Schweizer Archiv*, 37 (1971), 72–85

17. Rabus D., Deutung von Erstarrungsvorgängen in beliebigen realen Gusstücken mittels differenzierter technologischer Kalorimeterkurven. *Schweizer Archiv* 38 (1972), 79–88

18. Hribovsek B. & Marincek B., Einige Bemerkungen zur Erstarrungsgleichung. *Material und Technik*, (1973) 2, 69–71

19. Hribovsek B. & Marincek B., Bestimmung der gesamten freiwerdenden Wärme und des Kristallisationswärmeanteiles aus der Abkühlungskurve einer Schmelze. *Z. Metallkunde*, 65 (1974) 242–245

20. Takada H., An evaluation of the electroslag remelted ingot. *Proc. 2nd Int. Symp. on ESR, Mellon Inst, 1969*

21. Grünbaum G. & Gustafsson K., Electroslag remelting

22. Eisen W. B. & Campagna A., Computer simulation of consumable melted slabs. *Metall. Trans.* (1970) 849–856

23. Oeters F. & Sardemann K., Untersuchungen zum zeitlichen Verlauf der Erstarrung in der Randzone erstarrenden Eisens. *Arch. Eisenhüttenwes.*, 45 (1974) 8, 517–524

Carbon and low alloy steels

24. Kattamis T. & Flemings M. C., Dendrite Morphology, microsegregation and homogenisation of low alloy steels, *Trans. Met. Soc. AIME*, 1965, 5, 992–999

25. Ahearn P. J. & Quigley F. C., Dendritic morphology of high strength steel castings. *JISI*, 204 (1966) 16–22

26. Doherty R. D. & Melford D. A., Solidification and microsegregation in killed steel ingots with particular reference to 1% C 1.5% Cr-steel. *JISI*, (1966) 1131–1143

27. Tresh H. et al., Microsegregation in steel castings, *Trans. Met. Soc. AIME*, 242 (1968) 853–858

28. Suzuki A. et al., On secondary dendrite arm spacing in commercial carbon steels with different carbon content. *J. Japan Inst. of Metals*, (1968) 1301–1305

29. Rose A. & Boer H. & Hougardy H. P., Einfluss einiger Elemente auf die Kristallisation von Eisen bei der Erstarrung. *Arch. Eisenhüttenwes.* 39 (1968), 793–797

30. Flemings M. C. et al., Microsegregation in iron base alloys. *JISI*, 208 (1970) 371–381

31. Hammar Ö. & Grünbaum G., Influence of backdiffusion on microsegregation during solidification of low alloy steels. *Scand. J. Metallurgy.* 3 (1974) 11–20

32. Chuang Y. K. & Reinisch R. & Schwerdtfeger K., Kinetics of the diffusion controlled peritectic reaction during solidification of iron-carbon alloys. *Metall. Trans. A*, 6 (1975) 235–238

33. Steinmetz E. & Kast M., Vorgänge bei der schnellen Erstarrung von Eisen mit gelöstem Sauerstoff und Schwefel, *Arch Eisenhüttenw.* 46 (1975) 629–634

34. Ohashi T. et al., A study on solidification, segregation and fluid flow of molten steel in continuously cast slabs. *Trans ISIJ*, 15 (1975) 571–579

35. Edvardsson T. & Fredriksson H. & Svensson I., A study of the solidification process in low carbon manganese steels. *Metal Science*, 10 (1976) 298–306

36. Choudhury A. & Jauch R. & Löwenkamp H., Primärstruktur und Innenbeschaffenheit herkömmlicher und nach dem Elektro-Schlacke-Umschmelzverfahren hergestellter Blöcke. *Stahl u. Eisen*, 96 (1976) 946–951

37. Jacobi H. & Schwerdtfeger K., Dendrite morphology of steady state unidirectionally solidified steel. *Metall. Trans.*, A, 7(1976) 811–820

38. Clayton D. B. & Smith T. B. & Brown J. R., Application of electronprobe microanalysis to the study of micro segregation in a low alloy steel. *J. Inst. of Metals* 90 (1961–62) 224–228

39. Smith T. B., Microsegregation in low alloy steels. *Iron & Steel*, 37 (1964) 536–541

40. Philibert J. & Weinryb E. & Ancey M., A quantitative study of dendritic segregation in iron-base alloys with the electronprobe microanalyzer. *Metallurgie*, (1965) 203–211

41. Ward R. G., Effect of annealing on the dendritic segregation of manganese in steel. *JISI*, 194 (1956) 930–932

152

43. SchneidhoferA. & Plessing R. & Krainer E., Betriebser-fahrungen mit Elektroschlacke-Umschmelzanlagen. *Berg- u. Hüttenm. Mh*, 115, (1970), 11, 367–373

44. Hoffmeister H., Kristallseigerungen und eutektische Karbidausscheidungen in Eisen-Kohlenstoff-Molyb-dän-Legierungen. *Arch. Eisenhüttenw.*, 43 (1972) 689–692

45. Hoffmeister H., Kristallseigerungen und eutektische Karbidausscheidungen in Eisen-Kohlenstoff-Vana-din-Legierungen. *Arch. Eisenhüttenw.*, 44 (1973) 349–355

46. Chuang Y. K. & Wepner W. & Schwerdtfeger K., Be-rechnung der interdendritischen Anreicherung von Kohlenstoff und Sauerstoff bei der Erstarrung von Stahl. *Arch. Eisenhüttenw.* 44 (1973) 243–250

47. Fredriksson H. & Hellner L., The influence of carbon on the segregation of chromium in steel. *Scand. J. Metallurgy* 3 (1974), 61–68

48. Burns D. & Beech J., Blowhole formation during so-lidification of iron alloys. *Ironmaking and steelmaking (Quarterly)*, (1974) 4, 239–250

49. Fuchs E. G. & Roosz A., Homogenization of iron base cast alloys. *Metal Science*, 9 (1975) 111–118

50. Fredriksson H. & Stjerndahl J., On the formation of a liquid phase during cooling of steel. *Metall. Trans. B*, 6 (1975) 661–664

51. Ohide T. & Ohira G., The solidification structures of iron-carbon-phosphorous ternary alloys. *Brit. Foundryman*, 68 (1975) 4, 106–115

52. Bibby P. A. & Beech J., Solidification behaviour of low alloy steel castings, *JISI* 211 (1973), 290–292

53. Jacobi H. & Pitsch W., Untersuchung der Kristallisa-tionsabfolge bei der Erstarrung niedriglegierter Stäh-le, *Arch. Eisenhüttenw.* 46 (1975) 417–422

54. Schmidt L. & Fredriksson H., Formation of macro se-gregation and centre-line cracks in continuously cast steel. *Ironmaking and Steelmaking (Quarterly)*, 2 (1975) 61–67

Chromium steels

55. Subramanian S. V. & Haworth C. W. & Kirkwood D. H., Growth morphology and solute segregation in the solidification of some iron alloys. *JISI*, 206 (1968), 1027–1032

56. Staska E. & Blöch R. & Kulmberg A., Untersuchungen an Fe-Cr-C-Legierungen mit Zusätzen von karbidbil-denden Elementen. *Mikrochimica Acta*, (1970), suppl IV, 62–74

57. Barthel A. & Hoffmeister H. & Schürmann E., Einfluss der chemischen Zusammensetzung und der Abküh-lungsbedingungen auf den Gefügezustand von Guss-eisen mit rd. 3% C und 14% Cr für Walzen. *Arch. Eisenhüttenw.* 45 (1974) 795–801

58. Staska E. & Blöch R. & Kulmberg A., Untersuchungen an Fe-Cr-C-Legierungen mit Molybdänzusätzen. *Mikrochimica Acta*, (1974) suppl V, 111–127

59. Fredriksson H. & Brising S. & Remeus B., Studium av karbidutskiljning vid stelning av verktygsstål. Del II Kromstål. *Jernkontoret, Stockholm, Rep. D 114, 1975*

60. Hoffmeister H., Kristallseigerungen und primäre Kar-bidausscheidungen in chromlegierten gegossenen Werkzeugstählen. *Giessereiforschung*, 22 (1970), 3, 121–127

61. Straube H. & Blöch R. & Plöckinger E., Die Abhängig-keit der Kohlenstoffverteilung im Dreistoffsystem Eisen-Chrom-Kohlenstoff von der erstarrungsbeding-ten Kristallseigerung des Chroms. *Metall*. 29 (1975) 2

62. Fredriksson H., The mechanism of the peritectic reac-tion in iron-base alloys. *Metal Science*, 10 (1976) 77–86

63. Fredriksson H., Segregation phenomena in iron-base alloys. *Scand. J. Metallurgy*, 5 (1976), 27–32

64. Malm S., Influence of Si and Mn on the solidification of 1.5% C — 11% Cr-steels. *Scand. J. Metallurgy*, 5 (1976) 137–144

Stainless and heat resistant steels

65. Mayerhofer S. & Kohl H., Matematisch-statistische Untersuchungen über den Deltaferritgehalt bei au-stenitischen Stählen. *Berg- u. hüttenm. Mh*, 111 (1966) 9, 443–453

66. Guiraldenq P., Action alphagène et gammagène des principaux éléments d'addition dans les aciers inox-ydables nickel-chrome dérivés du type 18–10. *Mém. Sci. Rev. Mét.*, 64 (1967), 907–938

67. Kohl H., Der Delta-Ferritgehalt austenitischer Chrom-Nickel-Stähle im Gleichgewichts- und Un-gleichgewichtszustand. *Arch. Eisenhüttenw.* 40 (1969) 143–146

68. Lefevre I. & Tricot R. & Castro R., Ségregation et homogénéisation des aciers inoxydables austénitiqu-es. *Mém. Sci. Rev. Mét.*, 66 (1969) 517–529

69. Blanc G. & Tricot R., Solidification, ségrégation et homogénéisation des aciers inoxydables austénitiqu-es contenant de la ferrite delta. *Mém. Sci. Rev. Mét.*, 68 (1971), 735–753

70. von Fircks H. J., Glühtemperaturabhängige Bildung von δ-Ferrit in austenitisch-ferritischen Chrom-Nick-el-Stählen. *Neue Hütte*, 17 (1972) 210–215

71. Fredriksson H., The solidification sequence in an 18–8 stainless steel investigated by directional solidi-fication. *Metall. Trans.*, 3 (1972), 2989–2997

72. Masumoto J. et al., Einfluss der Primärkristallisation bei peritektischer Reaktion auf die Heissrissneigung von Stahlschweissgut. *Schweissen u. Schneiden*, 27 (1975), 450–454

73. Héritier J. & Lévy J., On the mechanisms of melting of Fe-Cr-Ni-alloys in the two-phase solid-liquid region. *Scripta Met.* 10 (1976), 107–110 or in *Mém. Sci. Rev. Met.* 73 (1976), 523–535

74. Däcker C. Å. & Fredriksson H., Föroreningars inverkan på varmsprickbenägenheten i rostfria stål. *Styr. f. tekn. utveckl. report, Stockholm*, March 1976

75. Schürmann E. & Brauckmann J., Untersuchungen über die Schmelzgleichgewichte in der Eisenecke des Dreistoffsystems Eisen-Chrom-Nickel. *Arch. Eisen-hüttenwes.* 48 (1977) 3–7

76. Leffler B. & Malm S., Volume changes accompanying solidification of some austenitic stainless steels. *Me-tals Technology* 4 (1977), 81–90

77. Schürmann E. & Voss H. J., Seigerungsverhalten der Legierungselemente in Eisen-Chrom-Nickel-Schmel-zen und bei Zusatz von Molybdän und Vanadin. *Arch. Eisenhüttenwes.* 48 (1977) 129–132

78. Hammar Ö. & Svensson U., The influence of steel composition on segregation and microstructure du-ring solidification of austenitic stainless steels. *Solidi-fication Conf., Sheffield*, 1977

79. Hoffmeister H., Kristallseigerung und Deltaferritbil-dung in austenitischem Schweissgut. *Schweisen u. Schneiden*, 25 (1973) 164–166

80. Siegel U. & Günzel M., Mikroseigerung in austeniti-schen Chrom-Nickel-Stählen, Teil I, *Neue Hütte* 18

81. Moharil D. B. & Jin I. & Purdy G. R., The effect of δ-ferrite formation on the post-solidification homogenization of alloy steels. *Metall. Trans,* 5 (1974), 59−63

82. Spies H. J., Beitrag zur Kennzeichnung erstarrungsbedingter Entmischungen in Stählen, *Neue Hütte,* 21 (1976) 344−348

83. Hull F. C., Delta ferrite and martensite formation in stainless steels. *Weld. J. Res. Suppl.,* 52 (1973) 193s−203s

84. Delong W. T., Ferrite in austenitic stainless steel weld metal. *Weld. Res. Suppl.* 53 (1974), 273s−286s

85. Åström H. et al., Hot cracking and microsegregation in 18−10 stainless steel welds. *Metal Science,* 10 (1976) 225−234

86. Thier H., Delta-Ferrit und Heissrisse beim Schweissen chemisch beständiger austenitischer Stähle. *Dtsch. Verlag für Schweisstechnik* (DVS) Düsseldorf 1976, 100−104

High speed steels

87. Kunze E. & Horn E., Zusammenhang zwischen Erstarrungsverlauf und Gefügeausbildung von Schnellarbeitsstählen. *DEW-Techn. Ber.* 1 (1961), 6−15

88. Brandis H. & Wiebking K., Einfluss einer Legierungsänderung beim Stahl S6-5-2 (Mo 20) auf seinen Erstarrungs- und Aufschmelzverlauf. *DEW-Techn. Ber.* 11 (1971), 139−146

89. Horn E. & Brandis H., Betrachtung zur Ausbildung der Phasen im Schnellarbeitsstahl S6-5-2 (Mo 20) mit abnehmendem Kohlenstoffgehalt. *DEW-Techn. Ber.* 11 (1971) 147−154

90. Bäckerud L. & Pfeifer H. U., Structure development in some tool steels during the solidification process. *Scand. J. Metallurgy* 1 (1972), 159−165

91. Barkalow R. & Kraft R. W. & Goldstein J. I., Solidification of M2 high speed steel. *Metall. Trans.* 3 (1972), 919−926

92. Galda E. J. & Kraft R. W., The effect of Mo and W on solidification of high speed steels. *Metall. Trans.,* 5 (1974), 1727−1733

93. Gunji K. et al., Solidification structure of high speed tool steel. *Trans. ISIJ,* 14 (1974), 257− 266

94. Fredriksson H. & Brising S., The formation of carbides during solidification of high speed steels. *Scand. J. Metallurgy,* 5 (1976), 268−275

95. Kulmburg A. & Wilmes S. & Korntheuer F., Zeit-Temperatur-Aufschmelzschaubilder einiger gebräuchlicher Schnellarbeitstähle. *Arch. Eisenhüttenwes.* 47 (1976) 319−324

96. Brandis H. & Wiebking K., Einfluss von Giesstemperatur und Erstarrungsverlauf auf die Gefügeausbildung von Schnellarbeitsstahl. *DEW-Techn. Ber.,* 11 (1971) 158−165

97. Mellberg P. O. & Sandberg H., Solidification studied by ESR remelting of high speed steel. *Scand. J. Metallurgy,* 2 (1973) 83−86

98. Sandberg H., Influence of titanium on micro segregations in high-speed steel ingots. *Scand. J. Metallurgy,* 2 (1973), 233−241

8. Alloy Index

Table 8.1 Index to the steels.

Table 8.2 a: Carbon and Low Alloy Steels, composition (wt-%).

Steel Number	C	Si	Mn	P	S	Cr	Ni	Mo	Cu	Al$_{tot}$	N	Others
Carbon:												
201	0,11	0,12	1,25	0,040	0,018	0,06	0,03	0,07	0,07	0,038	0,012	
202	0,12	0,27	1,53	0,010	0,005	0,02	0,03	$\leq$0,03	0,05	0,029	0,011	0,03Ce
203	0,18	0,44	1,26	0,016	0,025	0,01	0,02	0,06	0,02	0,004	0,007	0,03Nb
204	0,19	0,40	1,42	0,012	0,007	0,07	0,13	0,02	0,08	0,006	0,005	
205	0,36	0,27	0,58	0,015	0,012	0,08	0,05	0,02	0,12	0,004	0,007	
206	0,69	0,23	0,72	0,022	0,024	0,02	0,02	0,01	0,03	0,006	0,002	
207	1,01	0,25	0,46	0,012	0,009	0,02	0,03	0,02	0,03	$\leq$0,004	0,002	
Low Alloy:												
208	0,10	0,28	0,57	0,008	0,009	1,14	3,3	0,14	0,11	0,013	0,009	0,02 V
209	0,20	0,25	0,90	0,014	0,039	0,81	1,05	0,06	0,07	0,036	0,009	0,02 V
210	0,27	0,02	0,32	0,006	0,008	1,66	3,5	0,42	0,04	0,044	0,007	0,08 V
211	0,29	0,21	0,62	0,012	0,006	1,11	0,15	0,21	0,04	0,011	0,004	0,04 V
212	0,29	0,22	0,52	0,009	0,010	1,02	3,2	0,25	0,05	0,010	0,005	0,03 V
213	0,35	0,24	0,67	0,010	0,020	0,92	0,05	0,19	0,07	$\leq$0,004	0,008	0,02 V
214	0,52	0,22	0,85	0,010	0,006	1,07	0,07	0,07	0,04	$\leq$0,004	0,008	0,14 V
215	0,55	0,27	0,50	0,019	0,012	0,99	3,0	0,31	0,06	0,011	0,008	0,08 V
216	1,01	0,23	0,33	0,021	0,026	1,55	0,02	0,01	0,04	0,011	0,003	0,04 V

Table 8.2 b: Chromium Steels, composition (wt-%).

Steel Number	C	Si	Mn	P	S	Cr	Ni	Mo	Cu	W	V	Al$_{tot}$	N
301	0,13	0,36	0,37	0,003	0,007	5,0	0,01	0,58	0,02	0,01	0,01	0,009	0,006
302	0,35	1,03	0,46	0,020	0,007	5,2	0,23	1,34	0,11	0,09	1,0	0,013	0,026
303	0,50	1,00	0,48	0,025	0,010	5,1	0,18	1,36	0,10	0,02	1,20	0,013	0,036
304	0,96	0,29	0,67	0,020	0,015	5,2	0,13	1,19	0,09	0,05	0,21	0,014	0,024
305	0,04	0,54	0,61	0,010	0,009	13,4	5,5	0,07	0,07	0,01	0,01	0,019	0,032
306	0,07	0,54	0,48	0,020	0,006	12,9	0,17	0,02	0,10	0,01	$\leq$0,01	0,026	0,039
307	0,14	0,19	0,68	0,009	0,014	12,0	1,20	0,01	0,03	0,01	0,02	0,001	0,040
308	0,32	0,15	0,30	0,009	0,008	13,9	0,16	0,01	0,01	0,22	0,03	0,003	0,013
309	0,69	0,43	0,64	0,014	0,005	13,1	0,20	0,07	0,02	0,22	0,03	0,002	0,025

Table 8.2 c: Stainless and Heat Resistant Steels, composition (wt-%) and Cr-Ni equivalent ratios.*

Steel Number	C	Si	Mn	P	S	Cr	Ni	Mo	Cu	Co	Al$_{tot}$	N	Others	$\dfrac{Cr_{eq}}{Ni_{eq}}$
401	0,042	0,86	0,76	0,031	0,010	25,1	4,7	1,22	0,08	0,08	$\leq$0,002	0,077		4,01
402	0,012	0,31	1,76	0,008	0,008	19,8	9,9	0,10	0,04	0,02	0,004	0,031		1,82
403	0,019	0,31	0,94	0,009	0,010	19,5	10,2	0,11	0,03	0,05	0,002	0,044		1,74
404	0,036	0,44	1,25	0,025	0,010	18,4	9,1	0,38	0,20	0,25	0,002	0,081		1,68
405	0,068	0,59	1,44	0,028	0,001	17,2	10,3	0,47	0,24	0,27	0,048	0,005	0,51Ti	1,61
406	0,052	0,44	1,71	0,013	0,007	17,2	12,6	2,80	0,03	0,03	0,004	0,010	0,54Nb	1,58
407	0,023	0,53	1,58	0,020	0,006	17,2	13,5	2,63	0,19	0,07	0,004	0,031		1,43
408	0,048	0,63	1,65	0,018	0,007	17,7	13,4	2,68	0,15	0,07	0,004	0,045		1,42
409	0,024	0,58	1,79	0,009	0,011	17,4	12,8	2,77	0,03	0,03	0,002	0,20		1,32
410	0,008	0,24	1,77	0,009	0,008	25,1	22,2	2,3	0,02	0,02	0,002	0,067	0,08Ti	1,21
411	0,055	1,20	1,75	0,011	0,008	24,2	20,4	0,08	0,02	0,03	0,015	0,051	0,09Ti	1,15
412	0,13	0,52	1,67	0,009	0,003	24,3	20,5	0,11	0,03	0,04	0,023	0,053	0,08Ti	1,03
413	0,013	0,48	1,74	0,007	0,003	19,2	25,1	4,44	1,51	0,02	0,034	0,035	0,07Ti 0,07Ce	0,94
414	0,41	1,00	1,34	0,007	0,010	25,2	20,6	0,08	0,02	0,06	0,016	0,022	0,10Ti	0,89
415	0,07	0,62	0,56	0,007	0,003	21,1	30,9	0,06	0,02	0,02	0,39	0,019	0,40Ti	0,71

* Equivalents according to [78, 83] see chapter 6.

Table 8.2 d: High Speed Steels, composition (wt-%).

Steel Number	C	Si	Mn	P	S	Cr	Ni	Mo	Cu	Co	W	V	Al$_{tot}$	N
501	0,88	0,30	0,32	0,030	0,017	3,9	0,36	4,9	0,10	0,30	6,1	1,9	0,022	0,036
				0,010	0,037	3,8	0,14	9,2	0,11	0,05	1,5	2,0	0,010	0,036

Table 8.3 a: Carbon and Low Alloy Steels, liquidus and solidus temperatures and temperatures of formation of austenite and precipitates.

Steel Number	Type Analyses	Average Cooling Rate °C/s	Primary Phase	Temperatures, °C, of			
				Liquidus	Formation of Austenite	Formation of Precipitates	Solidus
Carbon:							
201	0,1 % C	2,0		1513	1476		1445
		0,5	δ	1513	1476		1450
		0,1		1515	1475		1455
202	0,12 % C	2,0		1514	1471		1440
		0,5	δ	1515	1475		1440
		0,1		1514	1477		1460
203	0,18 % C	2,0		1507	1467		1415
		0,5	δ	1506	1470		1430
		0,1		1507	1473		1460
204	0,2 % C	2,0		1503	1480		1425
		0,5	δ	1503	1477		1440
		0,1		1506	1480		1460
205	0,4 % C	2,0		1496	1479		1415
		0,5	δ	1498	1480		1425
		0,1		1501	1483		1440
206	0,7 % C	2,0		1471		1370-1335 Fe_3P-Fe_3C-	1335
		0,5	γ	1466		1370-1355-austenite	1355
		0,1		1474		1420-1370 eutectic	1370
207	1,0 % C	2,0		1457			1310
		0,5	γ	1457			1320
		0,1		1459			1340
Low Alloy:							
208	0,1 % C Cr Ni	2,0		1501	1485		1450
		0,5	δ	1501	1485		1450
		0,1		1502	1487		1465
209	0,2 % C Cr Ni	2,0		1502	1474	1460-1420	1420
		0,5	δ	1502	1474	1460-1425 MnS	1425
		0,1		1503	1465	-1445	1445
210	0,3 % C Cr Ni Mo	2,0		1487	1471		1395
		0,5	δ	1493	1490		1430
		0,1		1492	1490		1445
211	0,3 % C Cr Mo	2,0		1501	1460		1420
		0,5	δ	1501	1471		1435
		0,1		1503	1475		1450
212	0,3 % C Cr Ni Mo	2,0	γ	1486	—		1415
		0,5	δ	1487	1478		1425
		0,1	δ	1486	1477		1435
213	0,35 % C Cr Mo	2,0		1494	1479		1405
		0,5	δ	1493	1474		1415
		0,1		1495	1480		1425
214	0,5 % C Cr	2,0		1482			1380
		0,5	γ	1482			1385
		0,1		1483			1400
215	0,55 % C Cr Ni Mo	2,0		1471		1365-1335 carbide-	1335
		0,5	γ	1471		-1370 -austenite	1370
		0,1		1472		-1375 eutectic	1375
216	1,0 % C Cr	2,0		1450		1320-1270 Fe_3P-carbide-	1270
		0,5	γ	1450		1340-1300 -austenite	1300
		0,1		1451		-1300 eutectic	~ 1300

Table 8.3 b: Chromium Steels, liquidus and solidus temperatures and temperatures of formation of austenite and precipitates.

Steel Number	Type Analyses	Average Cooling Rate °C/s	Primary Phase	Liquidus	Temperatures, °C, of Formation of Austenite	Formation of Precipitates	Solidus
301	0,1 % C 5 % Cr	2,0		1508	1443		1405
		0,5	δ	1501	1426		1415
		0,1		1506	1444		1440
302	0,35 % C Mo V 5 % Cr	2,0		1471	1370		1335
		0,5	δ	1464	1387		1360
		0,1		1470	1412		1380
303	0,5 % C Mo V 5 % Cr	2,0		1460	1410	1320-1240 MC-	1140
		0,5	δ	1460	1410	1345-1300-austenite	1240
		0,1		1460	1412	-1320 eutectic	1260
304	1,0 % C Mo 5 % Cr	2,0		1435		1150-1130 M₇C₃ —	1130
		0,5	γ	1434		-1200-austenite	1200
		0,1		1438		-1215 eutectic	1215
305	0,04 % C 5 % Ni 13 % Cr	2,0		1470	1410		1355
		0,5	δ	1476	1419		1395
		0,1		1476	1425		1420
306	0,07 % C 13 % Cr	2,0		1497			1435
		0,5	δ	1500			1440
		0,1		1500			1455
		2,0				solid phase	1325-1270
		0,5				δ→γ	1330-1290
307	0,1 % C Ni 12 % Cr	2,0		1490	1416		1390
		0,5	δ	1495	1425		1400
		0,1		1494	1401		1400
308	0,3 % C 14 % Cr	2,0		1480	1400		1370
		0,5	δ	1483	1407		1375
		0,1		1482	1401		1390
309	0,7 % C 13 % Cr	2,0		1442	1414	1240-1195 M₇C₃-	1195
		0,5	δ	1448	1422	1250-1240-austenite	1240
		0,1		1444	1415	1260-1245 eutectic	1245

Table 8.3 d: High Speed Steels, liquidus and solidus temperatures and temperatures of formation of austenite and precipitates.

Steel Number	Type Analyses	Average Cooling Rate, °C/s	Primary Phase	Liquidus	Temperatures, °C, of Start of Formation of Austenite	Start of Formation of MC-Austenite Eutectic	Formation of Carbide -Austenite Eutectic	Solidus
501	0,9 % C 4 % Cr 5 % Mo	2,0		1414	1341	1260	1228	1175
	6 % W 2 % V	0,5	δ	1423	1342	1260	1232 M₂C + M₆C	1185
		0,1		1427	1350	1270	1255	1220
502	1,0 % C 4 % Cr 9 % Mo	2,0		1401	1305	—	1222	1175
	1,5 % W 2 % V	0,5	δ	1400	1315	—	1226 MC + M₂C	1180
		0,1		1400	1322	—	1233	1185

Table 8.3 c: Stainless and Heat Resistant Steels, liquidus and solidus temperatures and temperatures of formation of austenite and precipitates.

Steel Number	Type Analyses	Average Cooling Rate °C/s	Primary Phase	Liquidus	Formation of Austenite	Formation of Precipitates	Solidus
401	0,04 % C 25 % Cr 5 % Ni Mo	2,0		1465			1390
		0,5	δ	1471			1410
		0,1		1469			1420
402	0,01 % C 20 % Cr 10 % Ni	2,0		1447	1366		1325
		0,5	δ	1454	1391		1360
		0,1		1449	1405		1390
403	0,02 % C 19 % Cr 10 % Ni	2,0		1447	1404		1365
		0,5	δ	1455	1415		1390
		0,1		1453	1418		1405
404	0,04 % C 18 % Cr 9 % Ni	2,0		1452	1423		1365
		0,5	δ	1451	1409		1385
		0,1		1452	1424		1405
405	0,07 % C 17 % Cr 10 % Ni Ti	2,0		1436	1397		1335
		0,5	δ	1440	1406		1370
		0,1		1440	1412		1390
406	0,05 % C 17 % Cr 12 % Ni 2,8 % Mo Nb	2,0		1420	1410*	1330-1275 NbC-	1275
		0,5	$\delta + \gamma$	1423	1418*	1330-1290-austenite	1290
		0,1		1424	1417*	1330-1305 eutectic	1305
407	0,02 % C 17 % Cr 13 % Ni 2,5 % Mo	2,0		1423	1418*		1345
		0,5	$\delta + \gamma$	1427	1421*		1375
		0,1		1428	1425*		1380
408	0,05 % C 18 % Cr 13 % Ni 2,5 % Mo	2,0		1419	1414*		1330
		0,5	$\delta + \gamma$	1423	1422*		1360
		0,1		1421	1415*		1370
409	0,02 % C 17 %Cr 13 % Ni 2,5 % Mo 0,2 % N	2,0		1411			1310
		0,5	γ	1421			1350
		0,1		1422			1370
410	0,01 % C 25 % Cr 22 % Ni 2 % Mo	2,0		1401			1335
		0,5	γ	1402			1345
		0,1		1401			1355
411	0,07 % C 24 % Cr 20 % Ni	2,0		1399			1315
		0,5	γ	1401			1330
		0,1		1399			1350
412	0,1 % C 24 % Cr 20 % Ni	2,0		1405			1325
		0,5	γ	1407			1335
		0,1		1405			1355
413	0,01 % C 19 % Cr 25 % Ni 4 % Mo 1,5 % Cu	2,0		1389			1305
		0,5	γ	1391			1315
		0,1		1391			1345
414	0,4 % C 25 % Cr 20 % Ni	2,0		1383		1275-1260 $M_{23}C_6$-	1260
		0,5	γ	1385		1285-1275-austenite	1275
		0,1		1385		1290-1280 eutectic	1280
415	0,07 % C 21 % Cr 31 % Ni	2,0		1399		1305-1280 formation	1280
		0,5	γ	1401		1310-1295 of titanium	1295
		0,1		1400		1350-1330 compounds	1330

* The temperatures refer to the maximum rate of formation of austenite.

Table 8.4 a: Carbon and Low Alloy Steels, secondary dendrite arm spacings (μm).

Steel Number	Type Analyses	Partly Solidified Average Cooling Rate, °C/s	Completely Solidified Average Cooling Rate, °C/s		
		0,5	2,0	0,5	0,1
Carbon:					
201	0,1 % C	65	80	130	300
202	0,12 % C	70	85	200	390
203	0,18 % C	65	80	190	250
204	0,2 % C	85	75	120	230
205	0,4 % C	50	85	90	280
206	0,7 % C	70	75	130	160
207	1,0 % C	50	70	80	210
Low Alloy:					
208	0,1 % C Cr Ni	70	75	110	250
209	0,2 % C Cr Ni	60	85	110	180
210	0,3 % C Cr Ni Mo	60	70	90	160
211	0,3 % C Cr Mo	60	70	90	150
212	0,3 % C Cr Ni Mo	70	75	110	180
213	0,35 % C Cr Mo	65	80	100	190
214	0,5 % C Cr	55	75	90	140
215	0,55 % C Cr Ni Mo	65	70	90	130
216	1,0 % C Cr	60	75	90	140

Table 8.4 b: Chromium Steels, secondary dendrite arm spacings (μm).

Steel Number	Type Analyses	Partly Solidified Average Cooling Rate, °C/s	Completely Solidified Average Cooling Rate, °C/s		
		0,5	2,0	0,5	0,1
301	0,1 % C 5 % Cr	65	85	160	275
302	0,35 % C Mo V 5 % Cr	55	70	80	120
303	0,5 % C Mo V 5 % Cr	55	60	80	110
304	1,0 % C Mo 5 % Cr	55	65	80	110
305	0,04 % C 5 % Ni 13 % Cr	75	140	240	520
306	0,07 % C 13 % Cr	90	205	260	—
307	0,1 % C Ni 12 % Cr	75	150	180	470
308	0,3 % C 14 % Cr	75	75	100	210
309	0,7 % C 13 % Cr	50	65	80	130

Table 8.4 c: Stainless and Heat Resistant Steels, secondary dendrite arm spacings (μm).

Steel Number	Type Analyses	Partly Solidified Average Cooling Rate, °C/s	Completely Solidified Average Cooling Rate, °C/s		
		0,5	2,0	0,5	0,1
401	0,04 % C 25 % Cr 5 % Ni Mo	70	115	280	550
402	0,01 % C 20 % Cr 10 % Ni	60	150	270	450
403	0,02 % C 19 % Cr 10 % Ni	65	130	160	500
404	0,04 % C 18 % Cr 9 % Ni	40	125	190	340
405	0,07 % C 17 % Cr 10 % Ni Ti	50	85	110	200
406	0,05 % C 17 % Cr 12 % Ni 2,8 % Mo Nb	45	65	80	135
407	0,02 % C 17 % Cr 13 % Ni 2,5 % Mo	55	40	90	100
408	0,05 % C 18 % Cr 13 % Ni 2,5 % Mo	50	55	85	140
409	0,02 % C 17 % Cr 13 % Ni 2,5 % Mo 0,2 % N	40	45	70	105
410	0,01 % C 25 % Cr 22 % Ni 2 % Mo	60	60	80	160
411	0,07 % C 24 % Cr 20 % Ni	65	55	85	125
412	0,1 % C 24 % Cr 20 % Ni	60	65	90	125
413	0,01 % C 19 % Cr 25 % Ni 4 % Mo 1,5 % Cu	70	55	80	120
414	0,4 % C 25 % Cr 20 % Ni	60	50	80	105
		80	50	95	145

Table 8.4 d: High Speed Steels, secondary dendrite arm spacings (μm).

Steel Number	Type Analyses	Partly Solidified Average Cooling Rate, °C/s	Completely Solidified Average Cooling Rate, °C/s		
		0,5	2,0	0,5	0,1
501	0,9 % C 4 % Cr 5 % Mo 6 % W 2 % V	35	30	40	85
502	1,0 % C 4 % Cr 9 % Mo 1,5 % W 2 % V	35	25	35	70

Table 8.5 a: Carbon Steels, microsegregation in completely solidified samples, (average cooling rate 0,5°C/s).

Steel Number	Type Analyses	Element	I
201	0,1 % C	Mn	1,3
202	0,12 % C	Mn	1,4
203	0,18 % C	Mn	1,4
204	0,2 % C	Mn	1,6
205	0,4 % C	Mn	1,6
206	0,7 % C	Mn	1,7
207	1,0 % C	Mn	2,1

Table 8.5 b: Low Alloy Steels, microsegregation in completely solidified samples, (average cooling rate 0,5°C/s).

Steel Number	Type Analyses	Element	I
208	0,1 % C Cr Ni	Cr	1,3
		Ni	1,4
		Mo	2,5
209	0,2 % C Cr Ni	Cr	1,5
		Ni	1,4
210	0,3 % C Cr Ni Mo	Cr	1,6
		Ni	1,3
		Mo	2,2
		V	2,0
211	0,3 % C Cr Mo	Cr	1,6
		Mo	2,0
212	0,3 % C Cr Ni Mo	Cr	1,7
		Ni	1,4
		Mo	2,2
213	0,35 % C Cr Mo	Cr	1,5
		Mo	2,4
214	0,5 % C Cr	Cr	2,1
		V	1,9
215	0,55 % C Cr Ni Mo	Cr	2,1
		Ni	1,2
		Mo	2,5
		V	2,0
216	1,0 % C Cr	Cr	2,6

Table 8.5 c: Chromium Steels, microsegregation in completely solidified samples, (average cooling rate 0,5°C/s).

Steel Number	Type Analyses	Element	I
301	0,1 % C 5 % Cr	Cr	1,1
		Mo	1,4
302	0,35 % C Mo V 5 % Cr	Cr	1,2
		Ni	1,0
		Mo	1,5
		V	1,7
303	0,5 % C Mo V 5 % Cr	Cr	1,3
		Mo	1,5
		V	1,3
304	1 % C Mo 5 % Cr	Cr	1,4
		Mo	1,9
		V	1,7
305	0,04 % C 5 % Ni 13 % Cr	Cr	1,1
		Ni	1,2
306	0,07 % C 13 % Cr	Cr	1,0
		Ni	1,0
307	0,1 % C Ni 12 % Cr	Cr	1,1
		Ni	1,3
308	0,3 % C 14 % Cr	Cr	1,2
		Ni	1,0
309	0,7 % C 13 % Cr	Cr	1,2
		Ni	1,0

Table 8.5 e: High Speed Steels, microsegregation in completely solidified samples, (average cooling rate 0,5°C/s).

Steel Number	Type Analyses	Element	I
501	0,9 % C 4 % Cr 5 % Mo 6 % W 2 % V	Cr	1,6
		Mo	1,2
		W	0,8
		V	0,9
502	1,0 % C 4 % Cr 9 % Mo 1,5 % W 2 % V	Cr	1,8
		Mo	1,1
		W	0,6
		V	

Table 8.5 d: Stainless and Heat Resistant Steels, microsegregation in completely solidified samples, (average cooling rate 0,5°C/s).

Steel Number	Type Analyses	Element	I	P_D	P_{ID}
401	0,04 % C 25 % Cr 5 % Ni Mo	Mn	1,3		
		Cr	1,0		
		Ni	1,2		
		Mo	1,3		
402	0,01 % C 20 % Cr 10 % Ni	Si	1,7		
		Mn	1,4		
		Cr	1,0	1,2	
		Ni	1,5	0,7	
403	0,02 % C 19 % Cr 10 % Ni	Si	1,6		
		Mn	1,5		
		Cr	1,1	1,2	
		Ni	1,5	0,7	
404	0,04 % C 18 % Cr 9 % Ni	Mn	1,2		
		Cr	1,1	1,2	
		Ni	1,3	0,7	
405	0,07 % C 17 % Cr 10 % Ni Ti	Si	1,6		
		Mn	1,6		
		Cr	1,1	1,2	
		Ni	1,5	0,7	
406	0,05 % C 17 % Cr 12 % Ni 2,8 % Mo Nb	Si	1,7		
		Mn	1,5		
		Cr	1,1	1,3	1,1
		Ni	1,4	0,6	0,8
407	0,02 % C 17 % Cr 13 % Ni 2,5 % Mo	Mn	1,5		
		Cr	1,2		1,2
		Ni	1,2		0,8
		Mo	2,2		
408	0,05 % C 18 % Cr 13 % Ni 2,5 % Mo	Mn	1,6		
		Cr	1,2		1,2
		Ni	1,2		0,7
		Mo	2,1		
409	0,02 % C 17 % Cr 13 % Ni 2,5 % Mo 0,2 % N	Mn	1,6		
		Cr	1,2		
		Ni	1,1		
		Mo	2,1		
410	0,01 % C 25 % Cr 22 % Ni 2 % Mo	Mn	1,6		
		Cr	1,2		1,2
		Ni	1,1		0,8
		Mo	2,3		
411	0,07 % C 24 % Cr 20 % Ni	Si	2,4		
		Mn	1,9		
		Cr	1,2		
		Ni	1,2		
412	0,1 % C 24 % Cr 20 % Ni	Si	2,5		
		Mn	1,9		
		Cr	1,2		
		Ni	1,2		
413	0,01 % C 19 % Cr 25 % Ni 4 % Mo 1,5 % Cu	Si	1,8		
		Mn	1,7		
		Cr	1,2		
		Ni	1,1		
		Mo	2,0		
414	0,4 % C 25 % Cr 20 % Ni	Si	2,1		
		Mn	1,6		
		Cr	1,2		
		Ni	1,1		
415	0,07 % C 21 % Cr 31 % Ni	Si	2,3		
		Mn	1,7		
		Cr	1,2		
		Ni	1,1		

Table 8.6: Stainless and Heat Resistant Steels, formation of primary δ-ferrite and ferrite content in completely solidified samples at the solidus temperature and at 1200°C.

Steel Number	Type Analyses	Average Cooling Rate, °C/s	Solidified as Primary δ, %	Ferrite in Completely Solidified Sample, %
401	0,04 % C 25 % Cr 5 % Ni Mo	2,0	100	
		0,5	100	
		0,1	100	
402	0,01 % C 20 % Cr 10 % Ni	2,0	92	13
		0,5	91	19
		0,1	97	20
		0,5 (1200°C)		9
403	0,02 % C 19 % Cr 10 % Ni	2,0	91	11
		0,5	92	13
		0,1	98	9
		0,5 (1200°C)		5,8
404	0,04 % C 18 % Cr 9 % Ni	2,0	84	2,3
		0,5	82	4,7
		0,1	86	10
		0,5 (1200°C)		2,0
405	0,07 % C 17 % Cr 10 % Ni Ti	2,0	82	6
		0,5	82	8
		0,1	82	4,8
		0,5 (1200°C)		4,1
406	0,05 % C 17 % Cr 12 % Ni 2,8 % Mo Nb	2,0	< 60	4,0
		0,5	< 45	4,0
		0,1	< 42	3,9
		0,5 (1200°C)		2,9
407	0,02 % C 17 % Cr 13 % Ni 2,5 % Mo	2,0	< 46	5,5
		0,5	< 50	5,6
		0,1	< 34	4,4
		0,5 (1200°C)		3,5
408	0,05 % C 18 % Cr 13 % Ni 2,5 % Mo	2,0	< 36	4,0
		0,5	< 35	5,0
		0,1	< 34	5,5
		0,5 (1200°C)		0,1
409	0,02 % C 17 % Cr 13 % Ni 2,5 % Mo 0,2 % N	2,0	0	0,8
		0,5	0	0,8
		0,1	0	0,8
		0,5 (1200°C)		0,1
410	0,01 % C 25 % Cr 22 % Ni 2 % Mo	2,0	0	1,0
		0,5	0	1,0
		0,1	0	1,0
		0,5 (1200°C)		0,7
412	0,1 % C 24 % Cr 20 % Ni	2,0	0	0,5
		0,5	0	0,5
		0,1	0	0,5
		0,5 (1200°C)		0,4

Table 8.7: Chromium, Heat Resistant and High Speed Steels, carbide content in completely solidified samples (vol-%).

Steel Number	Type Analyses	Type of Carbide	Average Cooling Rate, °C/s		
			2,0	0,5	0,1
	Chromium Steel				
309	0,7 % C 13 % Cr	M_7C_3	4,5	3,5	2,4
	Heat Resistant Steel				
414	0,4 % C 25 % C 20 % Ni	$M_{23}C_6$	11,4	8,0 (1230°C)	7,2
				10,7 (1100°C)	
	High Speed Steels				
501	0,9 % C 4 % Cr 5 % Mo 6 % W 2 % V	$MC + M_2C + M_6C$		9	12
502	1,0 % C 4 % Cr 9 % Mo 1,5 % W 2 % V	$MC + M_2C$		9	10